**Daniela Maria Barata Rosa**

Licenciada em Química Aplicada – Biotecnologia

# Gold nanoparticulate systems for new anticancer compounds delivery

Dissertação para obtenção do Grau de Mestre em Genética Molecular e Biomedicina

Orientadora: Maria Alexandra Núncio de Carvalho Ramos Fernandes, Professora Doutora, FCT/UNL

Co-orientador: Pedro Miguel Ribeiro Viana Baptista, Professor associado com agregação, FCT/UNL

Júri:

Presidente: Prof. Doutora Ilda Maria Barros dos Santos Gomes Sanches

Arguente: Prof. Doutor Pedro Miguel Martinho Borralho

Vogal: Prof. Doutora Maria Alexandra Núncio de Carvalho Ramos Fernandes

FACULDADE DE CIÊNCIAS E TECNOLOGIA
UNIVERSIDADE NOVA DE LISBOA

**Setembro 2014**

My master studies have resulted in the following publication:

Martins P, Rosa D, Fernandes AR, Baptista PV. 2014. Nanoparticle Drug Delivery Systems: Recent Patents and Applications in Nanomedicine. *Recent Patents in Nanomedicine*. 3(2):105-118.

**GOLD NANOPARTICULATE SYSTEMS FOR NEW ANTICANCER COMPOUNDS DELIVERY**

## RESUMO

O cancro é responsável por mais de 8 milhões de mortes por ano a nível mundial. Apesar de ser uma das terapêuticas mais utilizadas, a quimioterapia não é totalmente eficaz devido aos mecanismos de resistência, intrínseca ou adquirida, aos fármacos por parte das células tumorais, e devido à grande toxicidade nas células saudáveis. O desenvolvimento de nanomateriais, *e.g*. nanopartículas de ouro (AuNPs), surge na procura de um tratamento mais eficaz para o cancro. As AuNPs são produzidas para libertar e aumentar a concentração dos fármacos dentro das células tumorais. O grande objectivo deste trabalho foi o desenvolvimento de sistemas baseados em AuNPs – AuNPs@PEG@BSA e AuNPs@PEG@HSA - para veicular dois compostos metálicos com potencial anti-proliferativo, $[Zn(Fendiona)_2]Cl_2$ e $[CoCl(H_2O)(Fendiona)_2]BF_4$, em linhas celulares de cancro colo-rectal (HCT116) e de cancro do pulmão (A549 e H1975). O desenvolvimento destes sistemas de AuNPs foi baseado na capacidade de interacção, anteriormente descrita, entre o composto TS265 e a HSA. As partículas e os nanoconjugados foram caracterizados por UV-Vis, TEM, DLS, ICP-MS, métodos de Bradford e de Ellman, permitindo confirmar a ligação das moléculas de PEG, BSA, HSA ou dos compostos à superfície. Os diâmetros hidrodinâmicos foram determinados por DLS em 83,01 ± 1,43 nm, 88,60 ± 5,80 nm, 76,21 ± 1,55 nm e 84,67 ± 1,68 nm para as AuNPs@PEG@BSA-TS262, AuNPs@PEG@BSA-TS265, AuNPs@PEG@HSA-TS262 e AuNPs@PEG@HSA-TS265, respectivamente. As AuNPs que continham o composto TS265 mostraram-se promissoras para o tratamento dos três tipos cancro testados, tendo a capacidade de reduzir a dose necessária de composto para atingir uma diminuição da viabilidade celular em 50 %. Em relação às AuNPs funcionalizadas com o composto TS262, apenas as AuNPs@PEG@HSA-TS262 se mostraram promissoras em HCT116.



**Termos-chave:** bioconjugação, células tumorais, citotoxicidade, libertação de drogas, nanopartículas de ouro, nanotransportadores de drogas

## ABSTRACT

Cancer is responsible for more than 8 million deaths worldwide per year. Although being widely used, chemotherapy is not completely effective due to drug resistance mechanisms, intrinsic or acquired by cancer cells, and due to the higher toxicity in healthy cells. The development of nanomaterials, *e.g.* gold nanoparticles (AuNPs), arises in demand of more effective cancer treatments. AuNPs are produced to delivery and enhance the drug concentration inside cancer cells. The main goal of this work was the development of AuNPs-based systems – AuNPs@PEG@BSA and AuNPs@PEG@HSA - for the vectorisation of two metallic compounds with anti-proliferative potential, $[Zn(Phendione)_2]Cl_2$ and $[CoCl(H_2O)(Phendione)_2]BF_4$ in colorectal cancer cell line (HCT116) and in lung cancer cell lines (A549 and H1975). The development of these AuNPs systems was based on the ability of the TS265 compound to interact with the HSA, previously described. The AuNPs and the nanoconjugates were characterised by UV-Vis, TEM, DLS, ICP-MS, Bradford and Ellman's assays, allowing the confirmation of the binding of the PEG, BSA and HSA molecules or the compounds on the surface. The hydrodynamic diameters were determined by DLS in 83.01 ± 1.43 nm, 88.60 ± 5.80 nm, 76.21 ± 1.55 nm and 84.67 ± 1.68 nm for AuNPs@PEG@BSA-TS262, AuNPs@PEG@BSA-TS265, AuNPs@PEG@HSA-TS262 and AuNPs@PEG@HSA-TS265, respectively. AuNPs containing the compound TS265 showed to be promising for the treatment of the three tested types of cancer, having the ability to reduce the required doses of the compound in which the cell viability decreases in 50 %. Regarding AuNPs functionalised with the compound TS262, only the AuNPs@PEG@HSA-TS262 showed to be promising in HCT116.

**Keywords:** bioconjugation, cancer cells, cytotoxicity, drug delivery, drug nanocarriers, gold nanoparticles

## SYMBOLS AND NOTATIONS

| | |
|---|---|
| % (m/v) | Mass/volume percentage |
| % (v/v) | Volume/volume percentage |
| A549 | Human lung carcinoma cell line (non-small cell lung cancer) |
| AuNPs | Gold nanoparticles |
| BSA | Bovine Serum Albumin |
| CCR | Complete Culture medium Recipe |
| Da | Dalton |
| DLS | Dynamic Light Scattering |
| DMEM | Dulbecco's Modified Eagle Medium |
| EDC | 1-ethyl-3-(3-dimethylaminopropyl) carbodiimide hydrochloride |
| EGFR | Epidermal Growth Factor Receptor |
| FBS | Fetal Bovine Serum |
| H1975 | Human lung adenocarcinoma cell line (non-small cell lung cancer) |
| $HAuCl_4$ | Chloroauric acid |
| HCl | Hydrochloride acid |
| HCT116 | Human colorectal carcinoma cell line |
| $HNO_3$ | Nitric acid |
| HSA | Human Serum Albumin |
| IARC | International Agency for Research on Cancer |
| $IC_{50}$ | Concentration of a drug at which cell viability decreases in 50 % in relation to the control |
| ICP-MS | Inductively Coupled Plasma Mass Spectrometry |
| MCF-10A | Healthy human cell line from mammary gland |
| MES | 2-(N-morpholino)ethanesulfonic acid |
| MTS | 3-(4,5-dimethylthiazol-2-yl)-5-(3-carboxymethoxyphenyl)-2-(4-sulfophenyl)-2H-tetrazolium |
| MW | Molecular Weight |
| $Na_2HPO_4$ | Sodium phosphate dibasic |
| NaCl | Sodium chloride |
| $NaH_2PO_4$ | Sodium phosphate monobasic |
| nm | Nanometres |
| PEG | Polyethylene glycol |
| Phendione | 1,10-phenanthroline-5,6-dione |
| PMS | Phenazine methosulfate |
| ROS | Reactive Oxygen Species |
| rpm | Rotations per minute |
| RPMI 1640 | Roswell Park Memorial Institute culture medium |
| RT | Room Temperature |
| SEM | Standard Error of the Mean |

| | |
|---|---|
| SPR | Surface Plasmon Resonance |
| Sulfo-NHS | N-hydroxysulfosuccinimide |
| TEM | Transmission Electron Microscopy |
| TS262 | $[Zn(phendione)_2]Cl_2$ |
| TS265 | $[Co(phendione)_2(H_2O)Cl]BF_4$ |
| UV | Ultraviolet |
| VEGF | Vascular Endothelial Growth Factor |
| Vis | Visible |
| WHO | World Health Organization |
| ε | Molar extinction coefficient |
| $\lambda_{em}$ | Emission wavelength |
| $\lambda_{exc}$ | Excitation wavelength |

## FIGURE INDEX

## TABLE INDEX

**TABLE OF CONTENTS**

# I. INTRODUCTION

## 1. CANCER

### 1.1 EPIDEMIOLOGY

Cancer is the leading cause of death in developed countries and the second leading cause of death in developing countries. Non-healthy life styles such as poor diets, not practicing sports or smoking addiction, are increasing the incidence of cancer mainly in economically developing countries (Jemal et al. 2011). According to the International Agency for Research on Cancer (IARC) there were 14.1 million new cancer cases worldwide in 2012, of which 6 million occurred in developed countries. In the same year there were 2.9 million cancer deaths in developed countries in a total of 8.2 million worldwide. (GLOBOCAN 2012)

In 2012, the most common cancer types in Portugal were breast, prostate, colorectal, lung, stomach and corpus uteri, causing a large number of cancer-associated deaths (GLOBOCAN 2012). According to GLOBOCAN, five of these were also the most frequent cancer types worldwide. A representation of the incidence and mortality rates for each of these cancer types is shown at Figures I.1A and I.1B, expressing how this affects the population in Portugal and all over the world.

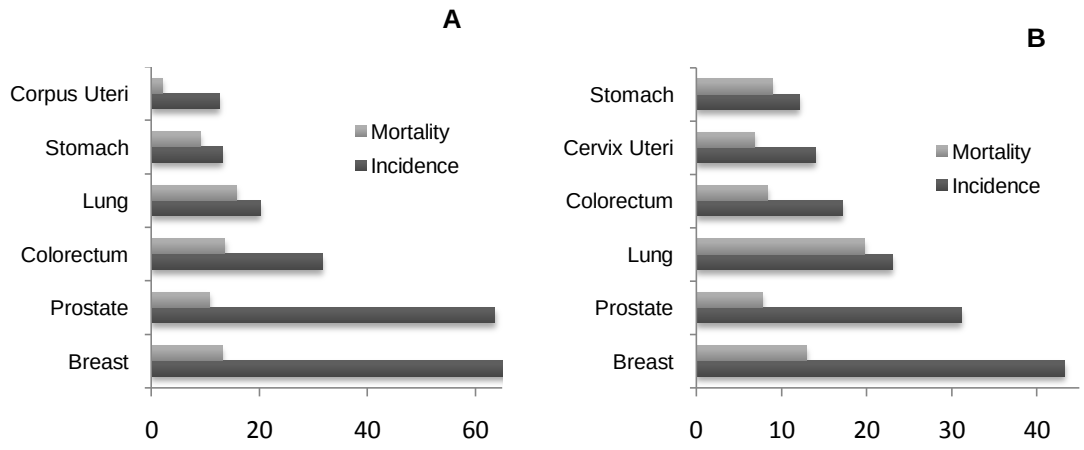


Figure I.1 - Estimated incidence and mortality rates for the most common cancer types in Portugal (A) and worldwide (B), per 100 000 persons in 2012. All ages and both sexes considered. Adapted from GLOBOCAN, 2012.

Estimated cancer incidence in the different continents, including both sexes and all ages, is represented at Figure I.2.

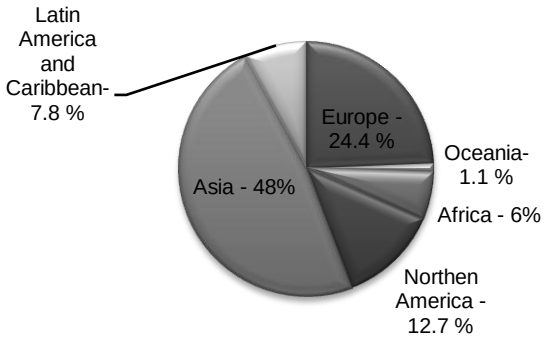


Figure I.2 – Percentage of incidence of new cancer cases by continent in 2012, excluding non-melanoma skin cancer. All ages and both sexes considered. Adapted from GLOBOCAN, 2012.

It is expected that annual cancer cases will rise from 14 million in 2012 to 22 within the next two decades (WHO – World Health Organization). Indeed, it is foreseen that in 2030, 21.7 million of new cancer cases worldwide will be diagnosed, of which 61000 in Portugal (GLOBOCAN 2012). Powerful economic countries will possibly show a slight mortality rate decrease towards 2030 due to early diagnosis and implementation of the newly developed cancer therapies (WHO).

## 1.2 CARCINOGENESIS

As seen in the previous section, cancer is a leading cause of death worldwide. This is a malignant disease defined as the rapid development of abnormal cells, their uncontrolled growth and spread, able to reach any part of the body via circulatory or lymphatic systems (WHO).

Carcinogenesis is a multistep process (Hanahan & Weinberg 2000, Lewis 2004, Negrini et al. 2010) in which normal cells undergo a progressive transformation to become malignant cells (Hanahan & Weinberg 2000). These steps reflect a series of genetic or epigenetic alterations that accumulate in genome (Lahtz & Pfeifer 2011, Negrini et al. 2013), causing genomic instability in almost all human cancers (Negrini et al. 2010). These alterations can be point mutations, small deletions or duplications, chromosomal rearrangements/translocations (Lahtz & Pfeifer 2011, Lewis 2004, Podlaha et al. 2012), or changes in DNA or histones by methylation or acetylation (Lal et al. 2013). Chromosomal instability is the major form of genomic instability observed in human malignant tumours (Negrini et al. 2010), and it was precisely the first type of genetic abnormality associated with cancer (Nowell & Hungerford 1960). It was observed that a translocation between chromosomes 9 and 22 (Philadelphia chromosome) was a critical step in chronic myeloid leukaemia patients. This translocation leads to the fusion of two protein kinases, the breakpoint cluster region (BCR) and Abelson leukaemia virus tyrosine kinase (ABL), which immortalises myeloid cells in the bone marrow, causing leukaemia (Lal et al. 2013).

Two classes of genes, proto-oncogenes and tumour-suppressor genes, play a key role in cancer induction. These genes encode proteins that help to control cell growth and proliferation;

loss of function of tumour-suppressors genes by inactivating mutations and/or the activation of proto-oncogenes by gain-of-function are strongly involved in the development of genomic instability in the cells, contributing to the development of cancer (Chow 2010, Lewis 2004, Yang et al. 2007). Mutations in these genes directly affect cellular integrity leading to uncontrolled cells proliferation, escape from apoptosis, and to an increase of spontaneous mutation rate (Chow 2010, Negrini et al. 2010) (Figure I.3). DNA repair genes are a third class of genes associated with abnormal cells development (Curtin 2012, Goode et al. 2002, Lahtz & Pfeifer 2011). The normal function of encoded proteins is to correct errors introduced in DNA by endogenous and/or exogenous mutagens (Goode et al. 2002). Thus, uncoordinated response of DNA repair genes leads to no DNA error correction, and consequently to carcinogenesis. Somatic mutations or epigenetic silencing of DNA repair genes are common in cancer (Curtin 2012). The normal functions of tumour suppressor and DNA repair genes are related and probably at the same level of importance regarding normal cell division and growth (Lahtz & Pfeifer 2011).

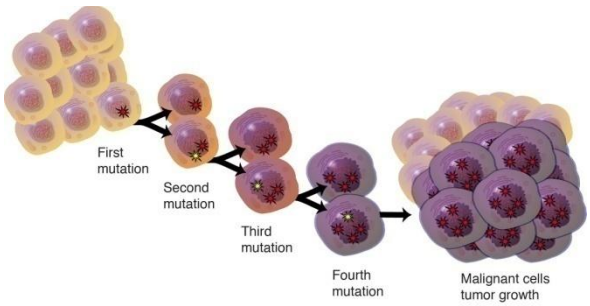


Figure I.3 – The accumulation of spontaneous mutations in genome, leading to cancer development. Cells acquire mutations in specific genes that control proliferation and all new generation of cells continue with these same mutations. More mutations can be acquired by these mutated cells leading to uncontrolled cell replication and cancer development (www.kintalk.org, accessed in March, 2014).

Consequently, the phenotype of cancer cells differs from normal cells, and in 2000 Hanahan & Weinberg identified six hallmark alterations in cancer cell physiology: i) stimulation of their own growth; ii) resistance to growth-inhibitory signals; iii) escape from apoptosis; iv) continuous proliferation; v) stimulation the growth of blood vessel to supply nutrients to tumours (angiogenesis) and vi) invasion of local tissue and spreading to distant sites (metastasis) (Hanahan & Weinberg 2000) (Figure I.4). Metastases are the main cause of death by cancer (WHO), with near 1500 deaths per day (Seyfried & Huysentruyt 2013). This process consists in the spread of cancer cells from the primary tumour to other subjacent or non-subjacent parts of the body, resulting in malignant secondary tumours (Seyfried & Huysentruyt 2013). Angiogenesis, defined as the formation of new blood vessels from pre-existing vessels (Ichihara et al. 2011), is necessary to support tumour survival and proliferation, supplying oxygen and nutrients to malignant cells, providing the opportunity for them to enter in the circulatory system and disseminate (Cooper 2000).

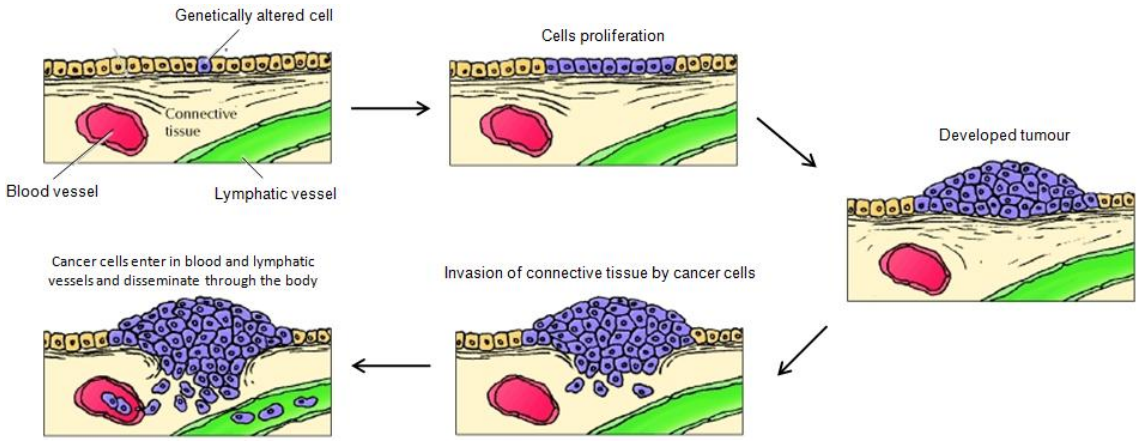


Figure I.4 – Development steps of a malignant tumour and dissemination of cancer cells through the body via capillary and lymphatic vessels. An altered cell at genetic level yields an uncontrolled proliferative cell population, leading to the onset benign tumour and then to cancer. Cancer cells may invade blood and lymphatic vessels which lead to metastasis. Adapted from Cooper, 2000.

In 2011, Hanahan & Weinberg updated the hallmarks of cancer and two new hallmark capabilities were included: reprogramming of energy metabolism and evading immune destruction (Hanahan & Weinberg 2011).

### 1.3 RISK FACTORS

Cancer result from genomic instability, but only 5 % of cancer cases are caused by internal factors, such as inherited mutations, defects in hormones or in immune system. Almost 95 % of cancer cases are caused by multiple mutations that result from population lifestyle and environment (Anand et al. 2008). Thus, some risk factors could be avoided, such as tobacco, alcohol abuse, poor diet, obesity or sedentary lifestyle, in order to not enhance the development of several cancer types (Anand et al. 2008, Irigaray et al. 2007). Although tobacco addiction in men has decreased significantly in several developed countries, it has increased progressively in women, remaining the main cause of cancer deaths (Irigaray et al. 2007). Tobacco contains at least 50 carcinogens (Anand et al. 2008), and besides lung cancer, is a risk factor for oesophagus, stomach, liver, bladder, kidney, cervical cancers and myeloid leukaemia (Anand et al. 2008, Irigaray et al. 2007). Environmental pollution, radiation and infectious microorganisms have also been implicated as causes of developing cancer. For instance, chronic infections caused by Human Papilloma Virus represent the main risk factor for cervix cancer development, and could also leading to carcinogenesis in vulva, vagina (Forman et al. 2012, Nygård et al. 2014), penis or anus (Forman et al. 2012). The second leading cause of cancer death is the development of malignant tumours in stomach (Selgrad et al. 2012), which also have a chronic infection as the main risk factor, caused by *Helicobacter pylori* (Selgrad et al. 2012, Wroblewski et al. 2010).

If cancer is early detected, a significant percentage of people can be cured by different cancer therapeutics (WHO).

## 1.4 THERAPEUTICS

The most common anticancer therapies consist of surgery, chemotherapy and radiotherapy, taken as conventional treatments by health care professionals (Irish Cancer Society, 2013). More recently emerged other types of cancer treatment such as the targeted therapy, photodynamic therapy, immunotherapy, or treatment by hyperthermia (American Cancer Society, 2013). The applied therapy depends on the type and stage of cancer. For instance, surgery and radiotherapy are more suitable for treating localised tumours, whereas chemotherapy is principally used when cancer cells spread outside their local of origin (Gordon & Nelson 2012). As a standard treatment and at different times, chemotherapy and radiotherapy could be also applied after malignant tumour removal by medical surgery (Cao et al. 2014).

### 1.4.1 CHEMOTHERAPY

Chemotherapy is defined by the use of one (monotherapy) or more therapeutic drugs (combined therapy) for cancer treatment (Cao et al. 2014). This type of therapy is in continuous development since the first drug was discovered, nitrogen mustard, by Louis Goodman and Alfred Gilman in 1942. Nitrogen mustard demonstrated for the first time the induction of tumour regression by chemotherapy in a patient with non-Hodgkin's lymphoma (Chabner & Jr 2005). Since then, research interest in anticancer drugs has increased and a significant number of these agents resulted in systemic therapeutics that cure or improve survival for certain cancer types (Gordon & Nelson 2012). The anticancer drugs should have a long half-life, high toxicity in cancer cells at biologically effective doses and should present high specificity for cancer cells (Chabner & Jr 2005). DNA-damaging drugs have been considered as the more advantageous in this process, causing cell cycle arrest and cell death (Helleday et al. 2008).

The major problems in chemotherapy are the low specificity of drugs for cancer cells, the serious toxic side effects, such as bone marrow suppression, mucositis and alopecia (Cao et al. 2014), and the ability of these abnormal cells to acquire resistance to anticancer drugs (Gordon & Nelson 2012). Drug resistance is precisely the main cause of treatment failure in metastatic cancer cases (Gordon & Nelson 2012, Hadjiandreou & Mitsis 2013, Longley & Johnston 2005), resulting from genetic mutations that may be intrinsic, reversible and dose-dependent or acquired during treatment (Hadjiandreou & Mitsis 2013).

Multidisciplinary researchers are required and collaborate together looking for more effective anticancer drugs, and ways to ensure their success in cancer treatment (Chabner & Jr 2005, Lal et al. 2013). Considering the knowledge on human cancer biology (Chabner & Jr 2005) and on anticancer drugs, the possibility of a better and personalised cancer therapy to each patient, depending on cancer type, is highly increasing (Lal et al. 2013, Longley & Johnston 2005). Targeted therapies strongly contribute for this revolution in cancer treatment. The response of cancer cells to chemotherapy can be modulated by this type of therapeutics, which are actually competing against drug resistance (Longley & Johnston 2005). The specificity of targeted

therapies to cancer cells is much higher, with fewer toxic effects on healthy cells (American Cancer Society, 2013). This topic is discussed in more detail in section I.2.1.

With the emergence of several new anticancer compounds, the organisation of chemotherapy drugs into classes became essential. Drugs are associated with each other considering their pathways and targets, their chemical structure and their activity when coupled with other drugs. According to American Cancer Society, chemotherapy drugs can be classified as alkylating agents, anti-metabolites, anti-tumour antibiotics, topoisomerase inhibitors, mitotic inhibitors, corticosteroids and miscellaneous. For instance, alkylating agents and anti-tumour antibiotics are both not phase-specific, *i.e.* act in all phases of the cell cycle, however alkylating agents work by damaging DNA whereas the anti-tumour antibiotics work by interfering with enzymes involved in DNA replication, dividing them into different classes (American Cancer Society, 2013).

#### 1.4.1.1 METAL COMPLEXES

A metal complex is defined by a central metal atom surrounded by a set of ligands. These ligands behave as Lewis bases, in which the atoms that form the bond to the central atom are named the electron donor atoms. The metal ion behaves as a Lewis acid in the complex, being the electron acceptor atom in bond formation (Atkins et al. 2010). Metal complexes are incessantly suggested as alternative drugs to current anticancer therapeutics. These complexes generally act as pro-drugs, which are modified by ligand exchange and redox processes before achieving the target site (Romero-Canelón & Sadler 2013).

The great interest in metal complexes as potential anticancer agents has increased since the discovery of biological activity of cisplatin [*cis*-diaminedichloroplatinum(II)] (Bharti & Singh 2009, Bruijnincx & Sadler 2008, Silva et al. 2013b). The mechanism of action of cisplatin is due to the formation of drug-DNA adducts, which interfere with replication and transcription processes, triggering cell cycle arrest and consequently apoptosis (Macciò & Madeddu 2013, Schmitt et al. 2012). This metallic drug is classified as an alkylating agent (American Cancer Society, 2013) and is the most remarkable chemotherapeutic agent that has been used in clinical medicine (Bharti & Singh 2009). As the majority of anticancer drugs, the use of cisplatin is restricted in cancer treatment due to dose-dependent toxic side effects, severe systemic toxicity and inherent or acquired drug resistance (Bruijnincx & Sadler 2008). This triggered the emergence of many other metal complexes (Martins et al. 2014a, Frezza et al. 2010) containing zinc, copper, gold (Frezza et al. 2010), ruthenium, arsenic, titanium, silver or rhodium as metal ions, with promising potential as anticancer drugs, having analogous or distinct mechanisms of action than cisplatin (Bharti & Singh 2009), such as the anti-proliferative activity against cancer cells or the inhibition of certain enzymes (Gianferrara et al. 2009).

Metal complexes provide a highly versatile platform for drug design due to their broad spectrum of coordination numbers and geometries, thermodynamic and kinetic characteristics

(*e.g*. strengths of metal-ligand bonds, redox potential or rates of ligand exchange (Romero-Canelón & Sadler 2013)), and intrinsic properties such as the type of metallic ion and the flexibility of containing several types of ligands (Bruijnincx & Sadler 2008). Take into account the classical chemotherapy, non-covalent interactions are the most frequently by metallic drugs, involving the intercalation of planar aromatic molecules between the base pairs of DNA, triggering cell death. Other mechanisms as the intercalation with RNA, cleavage of DNA strands and modifications of cell membrane functions have also been described regarding anticancer metallopharmaceuticals (Bharti & Singh 2009).

#### 1.4.1.1.1 TS262 AND TS265

The $[Zn(Phendione)_2]Cl_2$ (TS262) and $[CoCl(H_2O)(Phendione)_2]BF_4$ (TS265) complexes (Figures I.5A and I.5B, respectively) are two water-soluble metal-based compounds with cytotoxic activity against cancer cells (Luís et al. 2014, Silva et al. 2013a,b). For development studies and clinical progress concerning promising anticancer drugs, aqueous stability is a prerequisite (Pizarro et al. 2010). These anti-proliferative agents are both mononuclear compounds with zinc and cobalt as central metal atom, respectively (Silva et al. 2013b). TS262 is a homoleptic complex, meaning that all ligands in the complex are identical, which is in this case two 1,10-phenanthroline-5,6-dione (phendione) (Figure I.5C) bound to zinc(II). Relative to TS265, there are three different ligands, meaning that the complex is heteroleptic. Beyond the bidentate ligand phendione, there are a chlorine atom and a water molecule bound to cobalt(II) (Silva et al. 2013b).

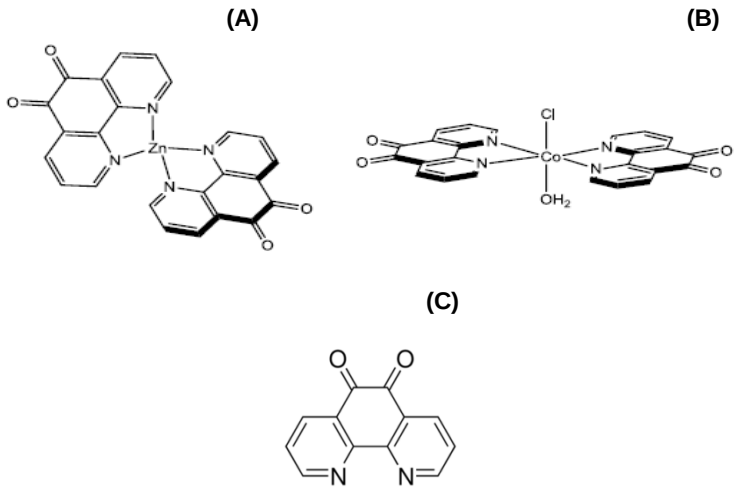


Figure I.5 – Chemical structure of the two anticancer metal complexes: (A) TS262 ($[Zn(phendione)_2]Cl_2$) and (B) TS265 ($[Co(phendione)_2(H_2O)Cl]BF_4$); and the structure of (C) 1,10-phenanthroline-5,6-dione (phendione), the ligand present in both TS262 and TS265 compounds (Silva et al. 2013b).

The anti-proliferative activity of TS262 and TS265 has been previously tested in HCT116 human colorectal carcinoma cell line and in healthy human fibroblast cell line and their $IC_{50}$ has been estimated (Silva et al. 2013b). $IC_{50}$ is a quantitative measure that consists in the

concentration of a drug at which cell viability decreases for 50 % in relation to the control, *i.e.* untreated cells. The *in vitro* anti-proliferative activities of TS262 and TS265 are lower in healthy human fibroblasts cell line (0.62 μM and 0.60 μM, respectively) than in HCT116 tumour cell line (0.217 ± 0.022 μM and 0.206 ± 0.023 μM, respectively), indicative of their slightly higher specificity for this type of cancer cells (Silva et al. 2013b). These estimated $IC_{50}$ values in HCT116 tumour cell line are about 70 times lower than the $IC_{50}$ values for the commonly used chemotherapeutic drug cisplatin (15.2 ± 0.55 μM), tested under the same conditions (Silva et al. 2013b). Other metal complexes bearing the ligand phendione with copper(II), silver(I) or manganese(II) as central metal atom have also shown promising anticancer potential even better than cisplatin against cancer cell lines (Bharti & Singh 2009). Moreover, anti-proliferative activity of TS265 has been also previously tested in healthy human cell line from mammary gland (MCF-10A) in which cell viability decreases only about 20 % at 1 μM of TS265, demonstrating once again the higher specificity for cancer cells than healthy cells (Luís et al. 2014). These positive features make it necessary a greater exploration of these metallodrugs as new potential compounds for cancer treatment.

TS265 complex has been more extensively studied than TS262. In recent studies was demonstrated that the anti-proliferative activity of TS265 is due to cell cycle arrest in S-phase and subsequent apoptosis (Luís et al. 2014, Silva et al. 2013a). Proteomic analysis of HCT116 cancer cells exposed to TS265 was also performed and it was observed the up-regulation of oxidative stress-related enzymes superoxide dismutase (SODC) and peroxiredoxine 2 (PRDX2), and also of stratifin (14-3-3 protein σ) and proliferation-associated protein 2G4 (PA2G4). An increased level of reactive oxygen species (ROS) was seen in the cells exposed at the same conditions, and the over-expression of SODC and PRDX2 are probably related with this fact because their function is precisely to protect cells from ROS. The formation of such ROS might arise from redox properties of TS265 complex. The down-regulation of translationally-controlled tumour protein (TCTP), heat shock protein beta 1 (HSPB1), endoplasmin (HSP90B1), tropomyosin 3 (TPM3), ezrin (EXRI) and cytoskeleton-related proteins, that are usually up-regulated in untreated cancer cells, was also observed in HCT116 cancer cells exposed to TS265 (Silva et al. 2013a). According to these results, the compound exhibits a great potential in the regulation of proteins that are typically deregulated in cancer cells. In order to study the interaction of TS265 with biological components circulating in blood of a living organism, the interaction between TS265 and human serum albumin (HSA) was studied, and results demonstrated a strong and specific interaction involving one binding site, near to Trp-214 (Luís et al. 2014). This suggests that the complex can be effectively transported by the most abundant protein in human blood plasma, a great influence for their distribution in the body. In fact, is reported the ability of complexes bearing the ligand phendione to bind covalently to proteins. The quinone moiety of phendione can behave as a nucleophile and react with the nucleophilic component in the side chains of lysine and arginine, *i.e.* the amino group and guanidine group (Yokoyama et al. 2006).

Similarly to TS262 complex, other metal compounds containing zinc as central metal atom have demonstrated to be potential non-classical anticancer agents, with new modes of action and new cellular targets compared to the classical chemotherapeutic drugs (Sanz Mendiguchia et al. 2013). It is believed that zinc is an important cytotoxic/tumour suppressor agent in several cancers since it was observed that the amount of cellular zinc was clearly lower (~60-80 %) in prostate cells cancer than in healthy or benign prostate cells. This relationship was proved for other types of cancer such as hepatocellular carcinoma, pancreatic adenocarcinoma, ovarian, oesophageal or colon cancers. The role of zinc on the inhibition of synthetic and energetic requirements for the malignant process, on the promotion of apoptosis and cell cycle arrest, and on the inhibition of invasion and migration prevents cancer development or, if cancer exist, the advancement to metastasis (Costello & Franklin 2012).

## 2. NANOMEDICINE

Nanomedicine is defined as the application of bionanotechnology to medicine (Yadav et al. 2011). In turn, bionanotechnology is defined as a fusion between two of the most promising technologies: biotechnology and nanotechnology. The objective of nanotechnology is the design, development and application of materials and tools at the nanoscale, *i.e.* ranging from 1 to 100 nm, whereas biotechnology uses the knowledge and techniques of biology to develop products and services based on molecular, genetic and cellular processes (Fakruddin et al. 2012). A broad range of areas are involved in this field, such as engineering, biology, medicine and chemistry, which are working together towards progress of bionanotechnology (Jabir et al. 2012). Bionanotechnology materials provide useful and direct applications in life sciences by sharing the same length scale of a great part of biomolecules (Kim et al. 2013) (Figure I.6).

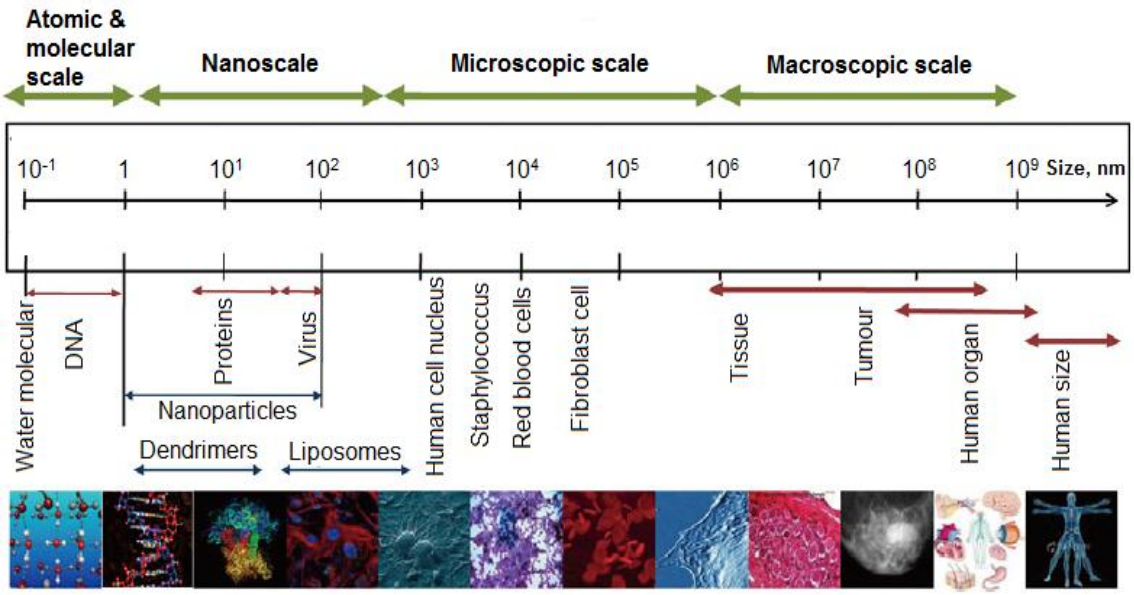


Figure I.6 – Multiple-scale of living biological materials and systems. Biomolecules of living systems and nanoscale materials share the same length scale providing an interface and direct applications of these materials in life sciences. Adapted from Kim et al. 2013.

Nanoparticles are the main focus in nanomedicine, be it for diagnostics or therapy, including selective targeting and molecular imaging for biomedical applications (Fakruddin et al. 2012, Parveen et al. 2012).

## 2.1 NANOPARTICULATE DRUG DELIVERY SYSTEMS IN CANCER TREATMENT

The application of functionalised nanoparticles, specifically in cancer biology, is a rapidly growing field, contributing to the development of methods for early detection of cancer cells (nanodiagnostics), and for the development of novel therapeutic approaches that enhances selectivity and efficacy of cancer therapy (Conde et al. 2014). In fact, besides cellular mechanisms of drug resistance, other of the main limitations of current chemotherapeutics is the inability to reach the target site, cell, tissue or organ, of therapeutic need (Martins et al. 2014b). Thus, biocompatible nanoparticles take advantage of the pathological and physiological conditions of cancer tissues, such as increase metabolism, local pH, enhanced permeability of endothelia, etc (Fakruddin et al. 2012). These nanomedicines may overcome limitations of traditional approaches in overcoming lack of selective targeting, gaining acess to tumour cells by surpassing biological, biophysical and biomedical barriers (Jabir et al. 2012).

The principle of targeted drug delivery system is the accumulation of drugs in the desired tissues, *i.e.* targeted site, reducing or eliminating deleterious side effects in healthy tissues (Silva et al. 2014c, Kumar et al. 2013a). Several types of nanoparticles, such as dendrimers, liposomes, carbon nanotubes, polymeric, ceramic and metallic nanoparticles are currently being used as targeted drug delivery systems for cancer treatment (Alexis et al. 2010, Wang et al. 2012). Therapeutic agents are encapsulated, entrapped, attached or dissolved in those nanoparticle-based systems and the targeted strategies for drug delivery may be achieved *via* passive or active mechanisms (Chakraborty et al. 2013). Passive strategy takes advantage of the pathophysiological features of diseased tissues that may be altered through the enhanced permeability and retention (EPR) effect. The leaky tumour blood vessels allow the circulating nanoparticles to easily accumulate in cancer tissues (Parveen et al. 2012). In turn, active targeting mechanisms are used to direct nanocarriers to specific sites utilising targeting moieties such as antibodies, lipoproteins, hormones, charged molecules or nucleic acids (Torchilin 2010). Thus, a better and personalised cancer treatment for each patient (previously discussed in section I.1.3), has started to be possible with the emergence of these nanoparticle-based drug delivery systems, improving the safety and efficacy of chemotherapeutics. Additionally to the advantages of deliver the drug at the desired site, nanocarriers systems fill other limitations of conventional chemotherapeutic agents, such as the administration of both hydrophilic and hydrophobic substances, decreased systemic toxicity and slower compound degradation, resulting in larger half-lives and consequently lower dosage (Martins et al. 2014b).

Despite intense research on biocompatible nanoparticles for cancer therapeutics, there are only a few nanoparticle systems for drug delivery approved by US Food and Drug Administration and

European Medicines Agency in the market: Caelyx®, Myocet®, DaunoXome®, DepoCyt®, Abraxane®, Genexol-PM® and Oncospar® (Egusquiaguirre et al. 2012).

### 2.1.1 GOLD NANOPARTICLES (AuNPs)

Among metallic nanoparticles available for medical applications, AuNPs are the most synthesised and explored nanocarriers (Martins et al. 2014b). AuNPs usually present themselves in colloidal suspension whose application and use dates back to ancient Rome, when they were used in stained glass for decorative purposes. However, the modern era of AuNPs began over 150 years ago when Michael Faraday observed that colloidal gold had different properties from bulk gold (Giljohann et al. 2010). In the 1950s, AuNPs began to be used in immunodiagnostics and histopathology, and were described as anti-neoplastic agents (Kumar et al. 2013b). In recent years there has been an increased interest in the attractive properties of colloidal gold, leading to new exciting developments with great potential in biology and medicine (Thompson 2007), being actually one of the most important candidates in the field of cancer therapy (Kumar et al. 2013b).

AuNPs present amazing optical properties derived from Surface Plasmon Resonance (SPR), resulting in high absorption and light scattering. Also their high chemical stability, low toxicity and biocompatibility make them a versatile vehicle, especially for drug delivery and imaging (Kumar et al. 2013a). The successful utilisation of AuNPs in biomedical assays is also dependent on the availability of methods to synthesise nanoparticles with controlled shape and size (1 to 150 nm in diameter). Perhaps the most used AuNPs of drug delivery systems are spherical with sizes between 20 and 60 nm, considered the therapeutic window for these nanovectors (Tiwari et al. 2011a) (Figure I.7). Colloidal solutions of gold nanospheres are typically red with the SPR band at ca. 520 nm, which depends from size alterations or refractive index of the surrounding media (Baptista et al. 2008).

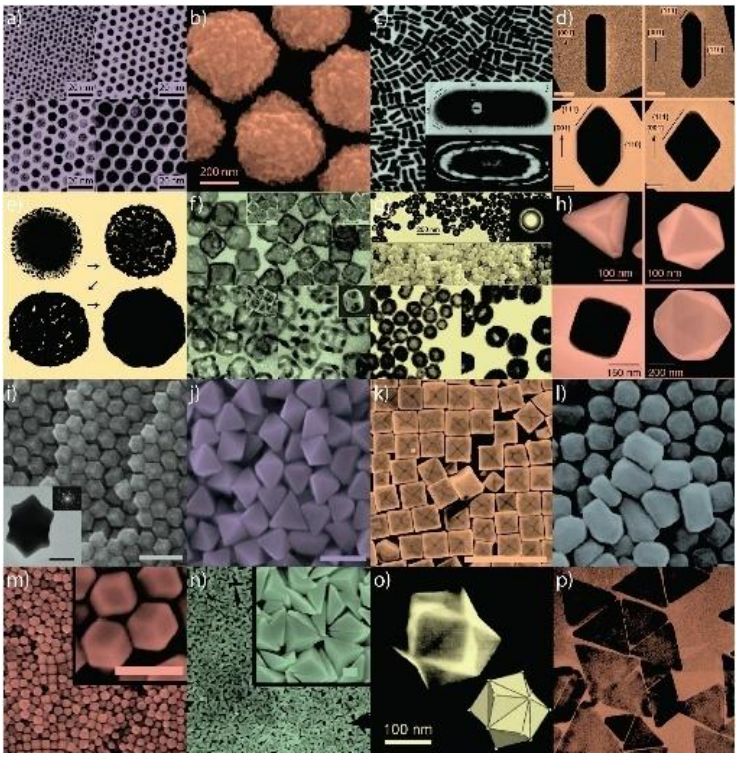


Figure I.7 – AuNPs of various size and shape with potential applications in biomedicine. Small (a) and large (b) nanospheres, (c) nanorods, (d) sharpened nanorods, (e) nanoshells, (f) nanocages/frames, (g) hollow nanospheres, (h) tetrahedra/octahedra/cubes/icosahedra, (i) rhombic dodecahedra, (j) octahedra, (k) concave nanocubes, (l) tetrahexahedra, (m) rhombic dodecahedra, (n) obtuse triangular bipyramids, (o) trisoctahedra, and (p) nanoprisms (Dreaden et al. 2012).

AuNPs can be easily modified with multiple surface moieties (*e.g.* PEG, BSA, oligo or polypeptides, oligonucleotides, antisense or sense RNA molecules, antibodies, cell surface receptors (Tiwari et al. 2011a)) and/or chemotherapeutic agents (Trivedi et al. 2012), in which the high surface-to-volume ratio offer an efficient drug loading capability – for a comprehensive review, please refer to Cabral & Baptista 2013, and references therein. The exceptionally optical properties arising from the SPR of AuNPs are affected by all of those modifications, and are reflected in wavelength alterations (Tiwari et al. 2011a) due to their higher sensitivity in optical detection methods (Baptista et al. 2008).

#### 2.1.1.1 SYNTHESIS

The first controlled synthesis of gold nanospheres was reported in 1951 by Turkevich et al. via the sodium citrate method in which monodisperse AuNPs (10-20 nm in diameter) were obtained. Later, Frens et al. optimised that method, and became the widely used method to produce AuNPs (Ladj et al. 2013). To synthesise AuNPs through this method, an aqueous solution of chloroauric acid ($HAuCl_4$) is used in which the $Au^{3+}$ ions are reduced to $Au^0$ by sodium citrate (Cai et al. 2008, Ladj et al. 2013). The ratio citrate/gold is the key to synthesise the particles with the desired size, wherein larger amounts of citrate promote the production of smaller gold nanospheres (Cai et al. 2008). The citrate has also the function of stabilise the

colloidal solution of gold, protecting AuNPs from aggregation (Ladj et al. 2013). Interestingly, AuNPs capped/stabilised with citrate ions are very convenient to be properly functionalised for biological applications due to the ease of binding molecules of interest directly to citrate ions or due to the ease replacement by other capping agents, *e.g.* thiolated capping agents (Baptista et al. 2008).

During the last few years many other interesting methods and techniques has been described for the synthesis of AuNPs such as microwave power, self reduction or the synthesis from microorganisms and plant extracts (Ladj et al. 2013).

#### 2.1.1.2 FUNCTIONALISATION

Functionalisation of AuNPs is essential for their efficacy in drug deliver, namely towards biocompatibility (DeLong et al. 2010) and long-term stability in biological fluids (Rahme et al. 2013). AuNPs should preserve their unique properties such as SPR absorption or light scattering with their functionalisation, and the bonded molecules should retain its biological recognition properties (DeLong et al. 2010). Molecules containing chemical functional groups, such as a polyethylene glycol (PEG) that holds a thiol and a carboxyl group, are normally used to stabilise AuNPs. One end of these molecules is strongly adsorbed on the gold surface by the thiol group. The other end stabilises the water-soluble nanoparticles by electrostatic repulsion of carboxylic acid or can be used for the conjugation of biomolecules to the AuNPs (DeLong et al. 2010) (Figure I.8). Please refer to Cabral & Baptista 2013 for additional insights.

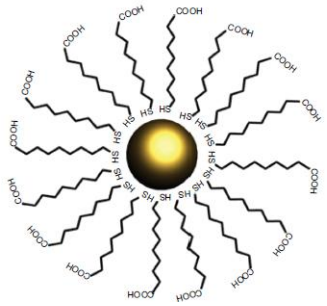

Figure I.8 – Adsorption of PEG molecules on an AuNP surface. One end of these molecules contains a thiol which is adsorbed on the gold surface, and the other end holds a carboxyl group that is facing toward the solution. This type of carbonate chains stabilise AuNPs against aggregation and allow their functionalisation with other biomolecules and/or chemotherapeutics (DeLong et al. 2010).

PEGylation, *i.e.* nanoparticles coated with PEG, is one of the mainly used methods that allow the stabilisation and functionalisation of AuNPs (Silva et al. 2014c, Tiwari et al. 2011b). The use of PEG enable the nanoparticles do not aggregate even under extreme pH or ionic strength conditions (DeLong et al. 2010). Furthermore, PEGylation has shown many other attractive properties such as the reduction of immunogenic response and the prevention of non-specific protein adsorption (Naahidi et al. 2013), increasing the stabilisation of AuNPs in biological environment, and also increasing the targeting and drug accumulation (Dreaden et al. 2012).

Regarding drug delivery systems, PEGylated nanoparticles have shown to slower chemotherapeutic agent degradation, thus extending their half-lives and decreasing the dosage (Naahidi et al. 2013).

There are various methods available for the conjugation of biofunctional molecules to AuNPs, and both physical and chemical mechanisms have been utilised. Among physical mechanisms, electrostatic interactions between a nanoparticle surface and an existing thiol group in the biomolecule are the most commonly, replacing some of the original stabiliser molecule (DeLong et al. 2010). Concerning chemical mechanisms, the most common method for AuNPs functionalisation consists in the covalent binding of amino groups on the biomolecules with free carboxyl groups at the end of the stabiliser molecule by using 1-ethyl-3-(3-dimethylaminopropyl) carbodiimide hydrochloride (EDC)/N-hydroxysulfosuccinimide (sulfo-NHS) coupling reaction (Figure I.9). EDC is a widely used carbodiimide that catalyses the reaction, and in turn, sulfo-NHS is used to stabilise the active intermediates by the formation of active ester functional groups with carboxylates (Bartczak & Kanaras 2011).

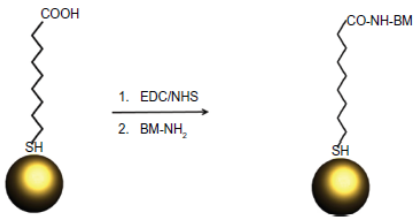


Figure I.9 – Scheme of chemical mechanism for the conjugation of biological molecules (BM) containing an amino group (-$NH_2$) to free carboxyl groups at the end of the stabiliser molecule on AuNPs, by EDC/sulfo-NHS mediated reaction (DeLong et al. 2010).

#### 2.1.1.3 AuNPs-BASED DRUG DELIVERY SYSTEMS FOR CANCER TREATMENT

Delivery of AuNPs into cells typically implies their adsorption onto cell surface followed by their internalisation, in which cell-penetrating peptides or cell surface antibodies coating AuNPs may facilitate their internalisation through endocytosis (Figure I.10). Endocytosis is the most prevalent mechanism used by cells to internalise this type of particles, however have been reported other mechanisms. Besides endocytosis, the internalisation of anionic AuNPs may also occur by forming an interface with the cell membrane when nanoparticles are coated with serum proteins, which are adsorbed by electrostatic and hydrophobic interactions. In turn, cationic AuNPs usually bind to negatively charged groups on the cell membrane and cross the plasma membrane. Despite those positively charged nanoparticles are the most effective in crossing cell membrane, show higher cytotoxicity than anionic or neutral AuNPs (Voliani et al. 2012).

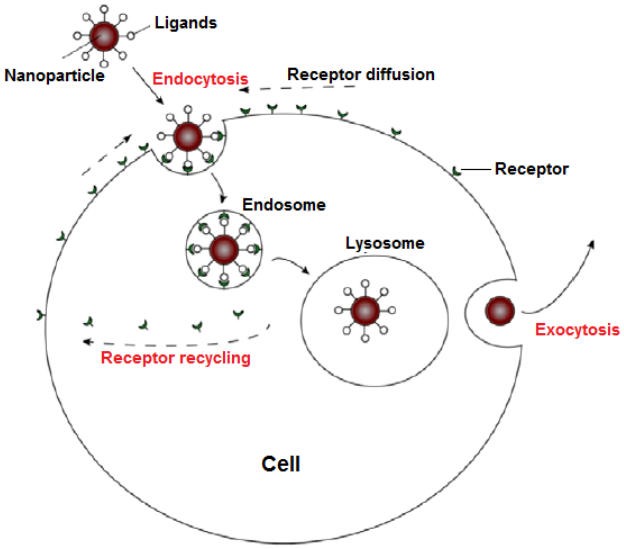


Figure I.10 – Representative scheme of the internalisation of AuNPs into cells through receptor-mediator endocytosis. In this representative case, AuNPs ligands bind to cell surface receptors and together are taken into the cell via endosomes. In this compartment, receptors and AuNPs ligands dissociate and follow two different pathways: cell surface receptors are recycled and AuNPs follow to lysosome, where every biofunctional molecules are degraded. By exocytosis, naked AuNPs are excluded from intracellular matrix. Adapted from Tran & Webster 2013.

AuNPs are functionalised with specific molecules to detect some stimulus (*e.g.* binding to a cell surface receptor, ionic concentration or pH media changes) in order to respond at once by releasing cargo, and consequently the drug, into cells or tissue *in vitro* and *in vivo* (Dreaden et al. 2012). Chemotherapeutic agents can be loaded into the cells by AuNPs through non-covalent interactions in which no structural modification is needed for drug delivery (Trivedi et al. 2012), in the case of hydrophobic drugs, or through covalent binding by coupling the terminal groups of the capping agents or the gold surface by affinity of thiols (Dreaden et al. 2012). In addition, and to address their success, these drug delivery nanosystems must be functionalised in order to carry the drug to the right place at the right time, overcoming all biological barriers (Kumar et al. 2013a).

The first formulation of AuNPs for cancer treatment in early-phase clinical trials is Aurimune™ (CYT-6091). This drug delivery system consists in 27 nm PEGylated nanoparticles bound to recombinant human tumour necrosis factor alpha (TNF-α), an anticancer agent, and has actually the phase I completed in clinical trials. Preclinical and clinical studies demonstrated the safety in humans through blood stream avoiding immune system, and a successful targeted delivery of TNF-α in solid cancers, at levels required for a biological response (CytImmune Sciences, Rockville).

Several formulations concerning AuNPs-based drug delivery systems for cancer treatment are being studied. Brown *et al*. developed an AuNPs-based system that improves the delivery and efficacy of oxaliplatin in cancer cells. They grafted oxaliplatin onto PEGylated AuNPs, showing

enhanced cytotoxicity in lung and colorectal cancer cell lines, and also an unusual ability to penetrate the nucleus in the lung cancer cells (Brown et al. 2010). Oxaliplatin, like the highly effective chemotherapeutic drug cisplatin, is known to be dose-dependent and represent dose-limiting severe side effects, like neurotoxicity, nausea and vomiting (Brown et al. 2010). Thus, in order to avoid compromising the therapeutic efficacy, it is important to develop of such nanosystems, avoiding the non-specific attack of all rapidly proliferating cells. Heo *et al*. also formulated a PEGylated AuNPs-based nanosystem that carries paclitaxel (Heo et al. 2012), one of the most effective chemotherapeutic drug, used for the treatment of several types of cancer (Ma & Mumper 2013). This drug delivery nanosystem demonstrated higher cytotoxicity in cancer cell lines than in normal cell lines, increasing their potential as an actively targeted anticancer drug (Heo et al. 2012). Also doxorubicin were tethered through disulfide linkage onto PEGylated AuNPs, and showed a significant inhibition of the growth of multidrug-resistant cancer cells *in vitro*. Doxorubicin is a topoisomerase inhibitor and an anthracycline antibiotic used for treating various types of cancer. However, the frequent clinical use of this chemotherapeutic agent often causes drug resistance and/or cardiotoxicity, highlighting the potential of these AuNPs-based drug delivery vehicles which overcome drug resistance in cancer treatment (Gu et al. 2012).

There are some formulations that demonstrate the advantage of using BSA on AuNPs for carrying drugs to the site of the disease. Murawala *et al.* have studied the effect of methotrexate on BSA capped AuNPs. They demonstrated that the functionalised AuNPs have higher cytotoxicity on breast cancer cell line compared with an equivalent dose of free methotrexate. The preferential uptake of nanoparticles by cancer cells was attributed to the presence of BSA on AuNPs that acts as a source of nutrient and energy for these malignant cells (Murawala et al. 2014). Methotrexate is an antimetabolite chemotherapeutic drug and prevents cells from using folate to make DNA and RNA, stopping the growth of cancer cells (American Cancer Society, 2011). AuNPs functionalised with BSA have been recently stated as one of the best drug delivery vehicle for cancer treatment (Khullar et al. 2012). Although many studies based on BSA-capped AuNPs have been reported, only a small number are reported with HSA on AuNPs surface.

The *in vivo* cytotoxicity of AuNPs functionalised with BSA or PEG molecules, with a thiol at one end and a carboxylic group at the other end (HS-PEG-COOH), were tested in mouse after intravenous injections. The study demonstrates that there was no statistical significance in the difference between the groups that receive the highest doses of AuNPs@BSA or AuNPs@PEG and the control group, *i.e.* untreated with nanoparticles. The mice in all groups were healthy, and were demonstrated by TEM images that the functionalised nanoparticles just accumulate in liver lysosomes. There was also no uptake in the nucleus, mitochondria or Golgi complex in liver cells, or in other cell types (Lien Nghiem et al. 2012). It was the first results of *in vivo* cytotoxicity studies concerning functionalised AuNPs with PEG or BSA, revealing two potential non-toxic vehicles for drug delivery.

## 3. OBJECTIVES

Numerous drug delivery nanosystems have been developed to improve the efficacy of chemotherapeutics and to target the drug to the desired cells, tissues or organs. The main goal of this work was to develop optimised AuNPs-based vehicles for drug delivery that could provide a solution to the afore mentioned problems. To achieve this goal several intermediate goals were set:

i) Cytotoxicity assays with free TS262 and TS265 in A549 and H1975 cancer cell lines, and the determination of the relative $IC_{50}$ of the compounds in these cell lines;

ii) Synthesis of AuNPs and subsequent functionalisation with PEG via Au-S covalent bond

iii) AuNPs@PEG functionalisation with BSA and HSA to obtain AuNPs@PEG@BSA and AuNPs@PEG@HSA;

iv) Assembly of AuNPs@PEG@BSA-TS262, AuNPs@PEG@BSA-TS265, AuNPs@PEG@HSA-TS262 and AuNPs@PEG@HSA-TS265;

v) Physic-chemical characterisation of the AuNPs systems;

vi) Cytotoxicity assays with AuNPs@PEG@BSA-TS262, AuNPs@PEG@BSA-TS265, AuNPs@PEG@HSA-TS262 and AuNPs@PEG@HSA-TS265 in HCT116, A549 and H1975 cancer cell lines

## II. MATERIALS AND METHODS

### 1. METALLIC COMPOUNDS – TS262 AND TS265

The metallic complexes, TS262 and TS265, used in the current work were synthesised at Area Departamental de Engenharia Química, ISEL, according to the methods described by Silva et al. 2013b. Stock solutions of TS262 and TS265 were prepared (10.1 mM and 23 mM, respectively) by dissolution in autoclaved milli-Q $H_2O$ (pH 7), and then aliquoted and stored at -20ºC. The chemical formula and molecular weight of the compounds are described in Table II.1.

Table II.1 – Required information to support the current work regarding compounds under consideration - TS262 and TS265.

| Compound | Chemical Formula | Molecular Weight (Da) | Solvent |
|---|---|---|---|
| TS262 | $ZnC_{24}H_{12}N_4O_4Cl_2$ | 617.9 | Autoclaved milli-Q $H_2O$ |
| TS265 | $CoC_{24}H_{14}N_4O_5BF_4$ | 619.6 | Autoclaved milli-Q $H_2O$ |

### 2. CULTURE OF HUMAN CELL LINES

HCT116 human colorectal carcinoma cells and A549 human lung carcinoma cells were grown in Dulbecco's Modified Eagle's Medium (DMEM) (DMEM, Invitrogen) supplemented with 10 % (v/v) Fetal Bovine Serum (FBS) (FBS, Invitrogen) and 1 % (v/v) antibiotic/antimycotic solution (*Pen-Strep+antimycotic:* 10000 units/mL of penicillin, 10000 µg/mL of streptomycin and 25 µg/mL of Fungizone® Antimycotic; Invitrogen), which is in conjunction nominated complete culture medium recipe (CCR). Cells were maintained in 75 $cm^2$ culture flasks (BD Biosciences) at 37 ºC in a 99 % humidified atmosphere of 5 % (v/v) $CO_2$ ($CO_2$ Incubator Leec, UK).

H1975 human lung adenocarcinoma cells was grown in RPMI (Roswell Park Memorial Institute) 1640 medium (RPMI; Invitrogen) supplemented with 10 % (v/v) FBS and 1 % (v/v) antibiotic/antimycotic solution (*Pen-Strep+antimycotic:* 10000 units/mL of penicillin, 10000 µg/mL of streptomycin and 25 µg/mL of Fungizone® Antimycotic; Invitrogen), which is also nominated CCR. As well as the cell lines previously described, these cells were maintained in 75 $cm^2$ BD flasks at 37 ºC in a 99 % humidified atmosphere of 5 % (v/v) $CO_2$.

At approximately 80 % of confluence, cell culture medium was renewed. For that, culture medium was aspired, added 4 ml trypsin (Invitrogen) and maintained for 5 minutes at 37 ºC in a 99 % humidified atmosphere of 5 % (v/v) $CO_2$. After confirming loss of cells adherence using an inverted microscope (Nikon TMS), 4 ml of appropriated CCR was added to the BD flask containing the cells to neutralise the trypsin. The solution was removed to a BD *Falcon* tube (BD Biosciences) and centrifuged for 5 minutes, at 1500 g and 15 ºC in a centrifuge (Sigma 3-16K, UK). Pellet was resuspended in 2 mL of the appropriate CCR medium, in which 50 µL of this solution was added to a new 75 $cm^2$ BD flask, contained 13 mL of CCR, and maintained in the

conditions previously described. The remaining cells suspension was used in the assays described in section II.3.2.

## 3. CYTOTOXICITY STUDIES OF TS262 AND TS265

### 3.1 CELL COUNT ASSAY BY TRYPAN BLUE

Cell count was assessed by trypan blue exclusion assay. A solution containing 100 µL of 0.4 % (m/v) trypan blue (Sigma), 350 µL of appropriate CCR to each culture and 50 µL of cellular suspension was placed on a haemocytometer (Hirschmann, Germany), and the number of viable cells was determined using an inverted microscope. After cell counting, cell density was determined according to Equation II.1:

(II.1)

$$\frac{Nr.of\ Viable\ Cells}{ml} = \frac{\Sigma Nr.of\ Viable\ Cells\ Quadrants\ 1\ to\ 4}{4}.10^4(Neubauer\ chamber\ volume\ in\ mm^3).Dilution\ Factor$$

### 3.2 CELL SEEDING WITH TS265 AND TS262

Following the determination of viable cells density, the cellular suspension obtained in section II.2 was diluted to 0.75 x $10^5$ cells/mL using the appropriated CCR. In a 96-well plate (Orange Scientific, Belgium) were seeded 7500 cells/well and incubated at 37 ºC in a 99 % humidified atmosphere of 5 % (v/v) $CO_2$ for 24 hours. After this time, cells seeded were observed using an inverted microscope and their adherence were confirmed. CCR was removed from each well and replaced by (i) 100 µL of fresh culture medium, the negative control, (ii) 100 µL of a range of concentrations of TS262 (0.1 – 40 µM), and (iii) 100 µL of a range of concentrations of TS265 (0.1 – 40 µM). The (ii) and (iii) solutions were prepared in fresh culture medium from the stock solutions of both compounds. All solutions were plating in triplicate. The 96-well plate was next incubated for 48 hours under the same conditions previously described.

### 3.3 CELL VIABILITY BY MTS ASSAY

After incubating the cells with the anticancer compounds for 48 hours (37 ºC in a 99 % humidified atmosphere of 5 % (v/v) $CO_2$), the cytotoxicity assay assessed by 3-(4,5-dimethylthiazol-2-yl)-5-(3-carboxymethoxyphenyl)-2-(4-sulfophenyl)-2H-tetrazolium (MTS) and phenazine methosulfate (PMS) (*CellTiter 96® Aqueous Non-Radioactive Cell Proliferation Assay*, Promega, USA) was performed. Culture medium was removed from each well of the plate and replaced by 100 µL of complete MTS solution per well (100:20:1 ratio of CCR, MTS and PMS, respectively). The 96-well plate was incubated for 30 minutes at 37 ºC in a 99 % humidified atmosphere of 5 % (v/v) $CO_2$.

MTS/PMS assay is a colorimetric method used for the quantification of viable cells. Viable cells are able to reduce MTS into a formazan product that absorbs at 490 nm. The absorbance at this

wavelength was measured directly from 96-well plates in a microplate photometer (Infinite M200, Tecan, Switzerland), and cell viability was determined according to Equation II.2:

(II.2)

$$Cell\ Viability\ (\%) = \frac{Absorbance\ at\ 490\ nm\ (sample)}{Absorbance\ at\ 490\ nm\ (negative\ control\ average)}.100$$

The percentage of cell viability for each concentration was determined take into account three independent assays.

### 3.4 RELATIVE $IC_{50}$

The relative $IC_{50}$, *i.e.* the quantitative measure that consists in the concentration of a drug at which cell viability decreases in 50 % compared to the control, was determined by *GraphPad Prism 6* program (GraphPad Software Inc., USA), take into account the three independent assays obtained in section II.3.3.

## 4. SYNTHESIS OF AuNPs

The colloidal solution of 14 nm AuNPs was prepared by the citrate reduction method, described by Lee and Meisel (Lee & Meisel 1982).

All glass materials used for the synthesis of AuNPs were previously immersed in *aqua regia* - prepared by adding 3 parts of concentrated HCl (Sigma) to 1 part of concentrated $HNO_3$ (Sigma) - for at least 2 hours, and after that, vigorously washed with milli-Q $H_2O$ (18.2 MΩ.cm at 25 °C). Thereafter, 250 mL of 1 mM $HAuCl_4$ (Sigma, MW 393.83 Da) was brought to a boil while stirring, in a 500 mL round-bottom flask. When in reflux, 25 mL of 38.8 mM of sodium citrate (Sigma, MW 294.10 Da) was added and kept refluxing for 20 minutes with continuous stirring. After this time, the colloidal solution was cooled to room temperature (RT), keeping the continuous stirring, and transferred to an Erlenmeyer flask and stored away from light at RT.

All solutions were prepared with milli-Q $H_2O$.

Hydrodynamic diameter of synthesised AuNPs was characterised by Transmission Electron Microscopy (TEM) and Dynamic Light Scattering (DLS), and their concentration determined by UV-Vis spectroscopy.

## 5. FUNCTIONALISATION OF AuNPs

### 5.1 AuNPs@PEG

AuNPs were functionalised with a bifunctional polyethylene glycol (PEG) molecule (Iris BIOTECH, MW 458.57 Da) containing a thiol group at one end of the molecule and a carboxyl group at the other end - HS-EG(8)-COOH.

In order to obtain a complete saturation of the polymer on AuNPs, a range of concentrations (0 - 0.1 mg/mL) of PEG were tested with a fixed concentration of nanoparticles. For that, different volumes of PEG were added to solutions containing 10 nM of synthesised colloidal AuNPs, 0.028 % of Sodium Dodecyl Sulfate (SDS) (Sigma, MW 288.38 Da) and milli-Q $H_2O$. These solutions were incubated for 16 hours while stirring in a GFL 3016 shaker at RT. Afterwards 16 hours incubation, all solutions were centrifuged at 14000 rpm for 30 minutes at 4 ºC, for three times to remove excess of PEG, where supernatants were removed to new eppendorfs and replaced by milli-Q $H_2O$. After obtaining all supernatants, those were also centrifuged at the same previously described conditions, and next thiolated chains of PEG present in these solutions were quantified by Ellman's assay.

Into each well of a 96-well plate was added 200 µL of each centrifuged supernatant, 100 µL of 0.5 M pH 7 phosphate buffer - prepared by the addition of 288.55 mM $Na_2HPO_4$ (Sigma, MW 141.96 Da) and 211.45 mM $NaH_2PO_4$ (Sigma, MW 119.98 Da) - and 7 µL of 2 mg/mL Ellman's reagent (5,5'-dithio-bis-(2-nitrobenzoic acid) - DTNB) (Sigma, MW 396.35 Da) prepared in 0.5 M pH 7 phosphate buffer, and next incubated at RT for 15 minutes. Absorbance was measured at 412 nm directly from 96-well plate in the microplate photometer. Under the same conditions, a linear standard curve was prepared in the range of 0 - 0.5 mg/mL of PEG, prepared in milli-Q $H_2O$, in which only the supernatant was replaced by 200 µL of PEG at different concentrations. Quantification of thiolated chains was determined after interpolation. Excess of PEG in solution indicated that saturation on the surface had been attained.

In the current work, the synthesised AuNPs were functionalised with 0.035 mg/mL of PEG.

Hydrodynamic diameter of synthesised AuNPs@PEG was characterised by DLS and their concentration determined by UV-Vis spectroscopy.

### 5.2 AuNPs@PEG@BSA

AuNPs@PEG were functionalised with Bovine Serum Albumin (BSA) (Sigma, MW 66,120 kDa) by a process based on a EDC/NHS reaction.

In order to obtain a complete saturation of BSA on AuNPs@PEG, a range of concentrations of BSA were tested with a fixed AuNPs@PEG concentration. For that, it was first prepared a master mix of 21 nM synthesised AuNPs@PEG, 1.25 mg/mL sulfo-NHS (Sigma, MW 217.13 Da) and 0.312 mg/mL EDC (Sigma, MW 191.70 Da) in 10 mM pH 6 MES buffer (2-(N-morpholino)ethanesulfonic acid) (Sigma, MW 195.24 Da). The master mix was incubated for 30 minutes and then the solution was centrifuged at 14000 rpm for 30 minutes at 4 ºC. The supernatant was removed and replaced by 2.5 mM pH 6 MES buffer, filling up to the original volume. The master mix was divided into equal volumes, and 0.2 mg/ml of BSA prepared in milli-Q $H_2O$ was added to attain the required range of concentrations (0 - 100 µg/mL). All solutions were incubated for 16 hours while stirring in a shaker, at RT.

Afterwards 16 hours incubation, solutions were centrifuged for three times at 14000 rpm for 30 minutes at 4 ºC to remove the excess BSA. Supernatants were removed to new eppendorfs and replaced by 2.5 mM pH 6 MES buffer after each centrifugation. Supernatants were also centrifuged at the same previous described conditions. Excess of BSA was quantified in the centrifuged supernatants by the Bradford assay. For that, to each well of a 96-well plate was added 150 µL of each centrifuged supernatant and 150 µL of Coomassie Brilliant Blue (*Coomasie Protein Assay Kit*, Thermo Scientific). After 15 minutes of incubation at RT, absorbance was measured at 450 and 595 nm directly from 96-well plate in the microplate photometer. Under the same conditions, a linear standard curve was prepared in the range of 0 – 100 µg/mL of BSA in milli-Q $H_2O$. In this case, 150 µL of BSA solutions at different concentrations and 150 µL of Coomassie Brilliant Blue were added to each well. Protein quantification in the supernatants was possible after interpolation in this standard curve. When BSA was detected in solution, it was known that the correspondent initial BSA concentration was sufficient to obtain the complete saturation of the protein on AuNPs@PEG. The ratio of the absorbance at 595 and 450 nm was utilised to obtain the linearisation of the standard curve, and thus Lambert-Beer law can be applied (Ernst & Zor 2010).

In the current work, the AuNPs@PEG were functionalised with 10 µg/mL of BSA.

Hydrodynamic diameter of synthesised AuNPs@PEG@BSA was characterised by DLS and their concentration determined by UV-Vis spectroscopy.

### 5.3 AuNPs@PEG@HSA

AuNPs@PEG were functionalised with Human Serum Albumin (HSA) (Sigma, MW 66,248 kDa) under the same conditions described in section II.5.2, in which BSA was replaced by HSA, and the protein concentration for the functionalisation of AuNPs@PEG was 30 µg/mL of HSA.

## 6. INCUBATION OF FUNCTIONALISED AuNPs WITH TS262 AND TS265

Solutions of 6 nM AuNPs@PEG@BSA and 6 nM AuNPs@PEG@HSA were mixed separately with 50 µM of TS265 or TS262 and incubated for 1 hour at 4ºC. After this period of time, solutions were centrifuged thrice at 14000 rpm for 30 minutes at 4 ºC, to remove excess of TS265 or TS262. Supernatants were replaced by autoclaved milli-Q $H_2O$.

All solutions were prepared in autoclaved milli-Q $H_2O$.

Quantification of TS265 or TS262 molecules linked to nanoparticles was performed by ICP-MS (Inductively Coupled Plasma Mass Spectrometry).

## 7. UV-VIS SPECTROSCOPY

Nanoparticle solutions were characterised using an UV-Vis spectrophotometer (UVmini-1240, Shimadzu, Germany). The absorbance measurements were made using 100 µL of volume quartz absorption cells (105.202-QS, Hellma, Germany). Spectra were normalised by shifting the baseline to zero.

## 8. TEM ANALYSIS

TEM was performed at Instituto de Ciência e Engenharia de Materiais e Superfícies at Instituto Superior Técnico (ICEMS/IST), Portugal – contracted service.

The samples were prepared by depositing 10 µL of the colloidal solution of gold in carbon copper grids, washing twice with milli-Q water, and air dried.

## 9. DLS ANALYSIS

The hydrodynamic diameter of nanoparticles was determined by DLS using a Nanoparticle Analyzer SZ-100 (Horiba Scientific, Japan) at 25 ºC, with a scattering angle of 90 º. Samples of 2 nM of AuNPs, AuNPs@PEG, AuNPs@PEG@BSA, AuNPs@PEG@HSA, AuNPs@PEG@BSA-TS262, AuNPs@PEG@BSA-TS265, AuNPs@PEG@HSA-TS262 or AuNPs@PEG@HSA-TS265 in milli-Q $H_2O$ were prepared. A total of 10 measures were taken for each sample.

## 10. ICP-MS ANALYSIS

Quantification of metals was assessed by ICP-MS, performed at Laboratório de Análises – Serviço de Espectroscopia de Emissão Atómica at Departamento de Química (DQ) at FCT-UNL – contracted service.

Samples were prepared by 200 µL aliquots of each solution, diluted in 1 mL of fresh *aqua regia*. All samples were measured in triplicate.

## 11. *IN VITRO* CYTOTOXICITY ASSAYS OF FUNCTIONALISED AuNPs

In a 96-well plate were seeded 7500 cells/well and incubated at 37 ºC in a 99 % humidified atmosphere of 5 % (v/v) $CO_2$ for 24 hours. After this time, cells seeded were observed using an inverted microscope and their adherence were confirmed. CCR was removed from each well and replaced by (i) 100 µL of fresh culture medium, the negative control (ii) 100 µL of AuNPs@PEG@BSA, (iii) 100 µL of AuNPs@PEG@BSA-TS262 and (iv) 100 µL of AuNPs@PEG@BSA-TS265. All solutions were prepared in fresh culture medium and plating in triplicate. The concentrations used in this assay correspond to relative $IC_{50}$ of free TS262 and

TS265 complexes in human cell lines, determined through *in vitro* cytotoxicity assay (see section II.3.4).

Under the same conditions, *in vitro* cytotoxicity assay was performed for AuNPs@PEG@HSA, AuNPs@PEG@HSA-TS262 and AuNPs@PEG@HSA-TS265.

After that, cells were incubated for 48 hours at 37 ºC in a 99 % humidified atmosphere of 5 % (v/v) $CO_2$. Subsequent to 48 hours incubation, cell viability was determined following the described protocol in section II.3.3.

## 12. STEADY-STATE FLUORESCENCE SPECTROSCOPY

Studies of the interaction between serum albumin and TS262 and TS265 were performed by steady-state fluorescence spectroscopy. The fluorescence intensity measurements were performed at RT using a Cary Eclipse Fluorescence spectrophotometer at excitation wavelength of 295 nm and recorded in the frequency range of 300 – 500 nm. BSA and HSA concentrations were kept constant (2.0 µM), and incubated with different concentrations of TS262 and TS265 (Table II.2):

Table II.2 – Range of concentrations of the metallic compounds TS262 and TS265 used for the incubation with BSA and HSA, to perform the fluorescence assays.

| | **TS262 (µM)** | **TS265 (µM)** |
|---|---|---|
| **BSA (2.0 µM)** | 0 – 400 | 0 - 375 |
| **HSA (2.0 µM)** | 0 - 90 | 0 - 130 |

BSA and HSA stock solutions were prepared in 10 mM pH 7.0 phosphate buffer with 0.15 M NaCl while TS262 and TS265 stock solutions were prepared in milli-Q $H_2O$. The samples of serum albumin and of each compound were mixed in order to obtain the desired concentrations and next incubated for 1 hour at 4 ºC, the same incubation time and temperature used in section II.6, before being analysed by fluorescence spectroscopy.

# III. RESULTS AND DISCUSSION

## 1. CYTOTOXIC POTENTIAL OF TS262 AND TS265

The *in vitro* studies in tumour cell lines are the initial step for the identification of new potential anticancer compounds. Only the compounds which are capable of significantly reduce tumour cell viability are selected as promising in cancer treatment.

TS262 and TS265 compounds were previously tested in a range of concentrations of 0.1 - 100 µM in HCT116 cell line (human colorectal carcinoma cell line), and there was a pronounced decrease in cell viability dependent on the increase of those concentrations (Luís 2011). Their previously reported anti-proliferative potential, prompted us, to continue the study of both compounds in HCT116 cell line. Two other tumour cell lines were also used for cytotoxicity studies of these compounds: A549 and H1975 cell lines, human lung carcinoma and human lung adenocarcinoma cells, respectively. Lung and colorectal cancers are the third and fourth most common cancer types in the world, respectively (GLOBOCAN, 2012).

The stock solutions of TS262 and TS265 were initially characterised by ICP-MS in order to quantify the zinc and cobalt atoms in both solutions, respectively. ICP-MS is one of the most utilised analytical techniques for the detection and quantification of small quantities of metals in solution (Stephan & Hineman 2012). From the results obtained it was concluded that the amount of zinc detected in TS262 samples was 2.14 ± 0.53 % higher and the amount of cobalt atoms in TS265 samples was 29.7 ± 0.45 % smaller than would be expected. According to these results, all compound concentrations were corrected in all assays shown below.

The evaluation of cytotoxicity of TS262 and TS265 in A549 and H1975 cell lines was performed by MTS assay. MTS is reduced into a formazan product, soluble in cell culture medium, by dehydrogenase enzymes found in metabolically active cells. Thus, the amount of formazan product, measured at 490 nm, is a measure of the metabolic viability of the cells which directly correlates with cell viability. The anticancer potential of TS262 and TS265 was tested on a range of increasing concentrations on both tumour cell lines, in which cells were exposed to compounds for 48 hours. The percentage of cell viability obtained for A549 and H1975 cell lines are represented in Figure III.1 and Figure III.2, respectively.

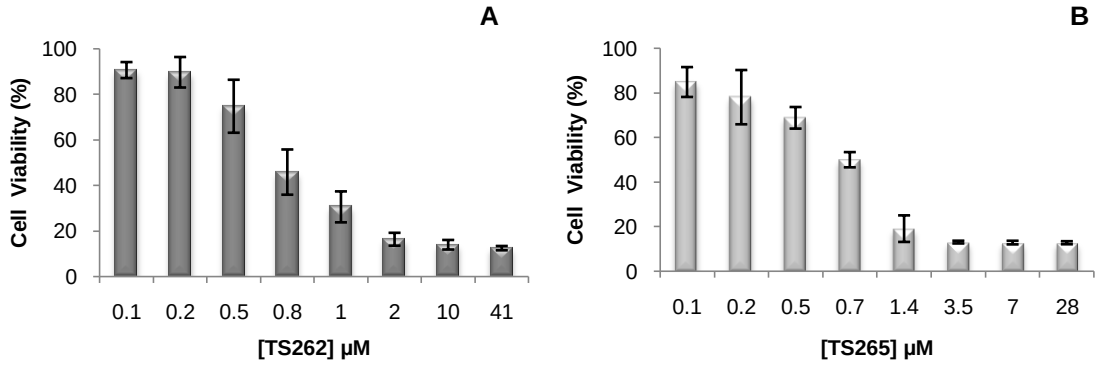


Figure III.1 – Cell viability in A549 human cell line obtained by MTS assay after exposure to (A) TS262 (0.1 – 41 µM) and (B) TS265 (0.1 – 28 µM) for 48 hours. Percentage of cell viability for each concentration is relative to the mean of three independent assays and error bars are correspondent to Standard Error of the Mean (SEM).

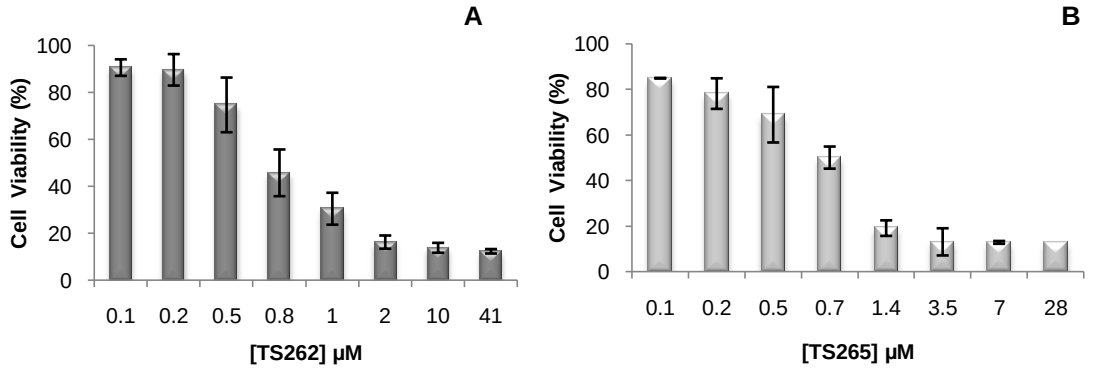


Figure III.2 – Cell viability in H1975 human cell line obtained by MTS assay after exposure to (A) TS262 (0.1 – 41 µM) and (B) TS265 (0.1 – 28 µM) for 48 hours. Percentage of cell viability for each concentration is relative to the mean of three independent assays and error bars are correspondent to SEM.

There was a decrease in cell viability in both A549 and H1975 cell lines, dependent on the increase of TS262 and TS265 concentrations, showing the great potential of these compounds as anti-proliferative agents. Based on these results it was determined the relative $IC_{50}$ values, that correspond to the required concentration of each compound to reduce cell viability in 50 %, compared to the control, *i.e.* untreated cells. For A549 cell line, the relative $IC_{50}$ values determined was 0.714 ± 0.091 µM for TS262 and 0.741 ± 0.007 µM for TS265. In the case of H1975 cell line, the relative $IC_{50}$ values are also similar for both compounds: 0.355 ± 0.038 µM for TS262 and 0.349 ± 0.021 µM for TS265. Despite the similar $IC_{50}$ values, both compounds show higher *in vitro* anti-proliferative activities for H1975 cancer cell line.

Previously, our laboratory has reported $IC_{50}$ values in HCT116 cell line of 0.217 ± 0.022 µM for TS262 and 0.206 ± 0.023 µM for TS265, under the same conditions (Silva et al. 2013b). The *in vitro* anti-proliferative activities of TS262 and TS265 were also tested in healthy human fibroblasts, demonstrating a higher (3.5x) anti-proliferative activity towards HCT116 cancer cells compared to fibroblasts ($IC_{50}$ values determined in 0.62 µM and 0.60 µM for TS262 and TS265, respectively) (Luís et al. 2014). This increased selectivity for normal cells was also observed

when compared their activity in H1975 cancer cells with the activity in healthy fibroblasts cells. However, the same behaviour was not observed when compared with A549 cancer cells. The TS265 was also tested in MCF-10A, a normal human epithelial cell line from mammary gland, and your relative $IC_{50}$ value was determined in 5.14 ± 0.01 μM (Luís et al. 2014). This value is much higher than all relative $IC_{50}$ values determined for TS265 in the three epithelia type cancer cell lines: HCT116, A549 and H1975. These results clearly show that both compounds are much more cytotoxic to the three cancer cells when compared to normal epithelial cells. Nevertheless, their $IC_{50}$ values in normal fibroblasts indicate that for reducing cellular toxicity *in vivo,* they should be targeted towards cancer cells. The viability assay in MCF-10A cell line should be also performed for TS262 compound.

## 2. SYNTHESIS AND CHARACTERISATION OF AuNPs

AuNPs have been proposed for cancer treatment based on their great advantages as a vehicle for drug delivery. In particular, AuNPs due to their straightforward synthesis with size and shape control, accessible methods for their characterisation, easily surface functionalisation and the ability to penetrate into tumour cells in *in vitro* assays have been widely used (Silva et al. 2014c).

AuNPs were successfully synthesised by the reduction of $HAuCl_4$ solution with sodium citrate, characterised by UV-Vis spectroscopy, TEM and DLS, and used throughout this study. UV-Vis spectroscopy is the most common used method for characterise the optical properties of AuNPs due to the SPR band of colloidal gold (Shi et al. 2012). This SPR band is strongly dependent on the size, shape, dispersity and local environment of the nanoparticles (Abdelhalim et al. 2011, Shi et al. 2012). Figure III.3A shows the UV-Vis absorption spectra of the synthesised AuNPs at a pH 7.0 solution. A symmetric absorption peak, indicative of monodisperse and spherical nanoparticles (Shi et al. 2012), is observed at 519 nm, typical of this type of AuNPs, *i.e*. with an approximate diameter of 14 nm (Lien Nghiem et al. 2012). The colloidal gold concentration could be also calculated based on this absorption spectrum by the Lambert-Beer law, assuming a molar absorptivity for the plasmon resonance band maximum of $2.33 \times 10^8$ $M^{-1}cm^{-1}$ (Baptista et al. 2005, Conde et al. 2012b). The expected usual concentration in this type of synthesis should be ~14 nM of AuNPs (Conde et al. 2012b).

TEM has been also found to be a powerful tool for the characterisation of AuNPs, providing direct visualisation of the morphology and size distribution of nanoparticles (Murawska et al. 2012). The TEM results (Figure III.3B) confirmed the great monodispersion of AuNPs and their spherical shape. The average particle size was also determined from TEM images with a mean diameter of 14.26 ± 0.31 nm. These results were in agreement with the UV-Vis results.

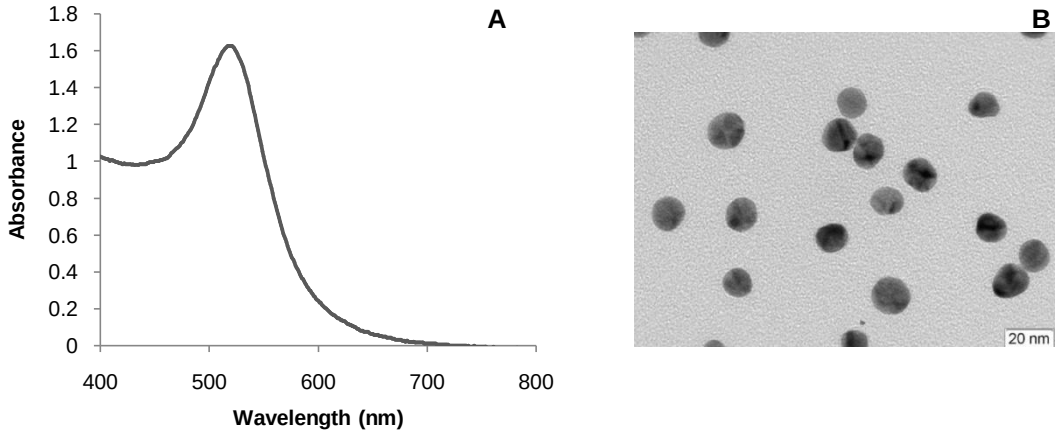


Figure III.3 – Characterisation of the synthesised AuNPs with the mean diameter of about 14 nm by (A) UV-Vis spectroscopy in the wavelength range of 400 - 800 nm (pH 7.0), and (B) TEM (scale bar: 20 nm).

Characterisation through DLS can also give powerful and complementary information about AuNPs. In this technique, small particles in suspension undergo random thermal motion known as Brownian motion, which is directly related to the AuNPs hydrodynamic diameter. The determination of nanoparticles hydrodynamic diameter was computed from the intensity of the scattered light and processed by the instrument software, based on the theory of Brownian motion and Stokes-Einstein equation (Equation III.1) (Dynamic Light Scattering, HORIBA Scientific, 2014):

(III.1) $$D_h = \frac{k_B T}{3\pi\eta D_t}$$

, where $D_h$ is the hydrodynamic diameter, $k_B$ the Boltzmann's constant, T the thermodynamic temperature, $D_t$ is the translational diffusion coefficient and η is the dynamic viscosity. The DLS results revealed an AuNPs average hydrodynamic diameter of 14.14 ± 0.43 nm. This method also confirmed the expected size of nanoparticles.

## 3. CHARACTERISATION OF FUNCTIONALISED AuNPs

### 3.1 AuNPs@PEG

The prepared AuNPs were then coated with PEG molecules to increase their stability and biocompatibility, and also provide the chemical functionality of further derivatisation. Figure III.4 (red line) shows the UV-Vis absorption spectrum of the stabilised AuNPs@PEG. The plasmon absorption peak of naked AuNPs (see black line, Figure III.4) clearly shifts from 519 to 522 nm after their functionalisation with PEG. This shift means that there was a change in the nature surrounding the AuNPs, confirming the Au-S covalent bond between nanoparticles and PEG.

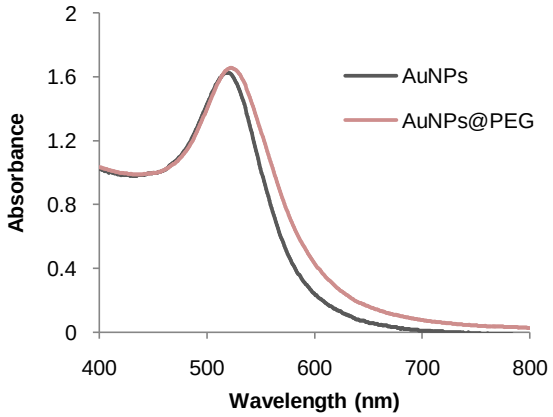


Figure III.4 – Spectra of the previous synthesised AuNPs and AuNPs@PEG obtained by UV-Vis spectroscopy, in the wavelength range of 400 - 800 nm (pH 7.0).

Figure III.4 shows a constant absorption spectrum of AuNPs@PEG meaning that the amount of PEG utilised (0.035 mg/ml) to cover the entire surface of AuNPs was capable to maintained these nanosystem stable in a pH 7 solution (milli-Q $H_2O$). The amount of thiolated chains covalently bounded to each AuNP was determined by Ellman's method (Figure VI.1, appendices). A AuNP:PEG ratio of 1:5591 (± 157) was obtained. These results were in agreement with previous studies, in which AuNPs with a hydrodynamic diameter of 14.47 nm were covered with a dense layer of PEG (MW = 458.57 Da), wherein a AuNP:PEG ratio of 1:5624 was calculated (Conde et al. 2012a).

The AuNPs modified surface was also characterised through DLS with an average hydrodynamic diameter determined on 35.20 ± 1.26 nm. There was clearly an increase on particle size of about 20 nm when the citrate ions were replaced by PEG molecules. It is thought that there was a triple layer of PEG capping AuNPs since each PEG molecule size is 3.25 nm (http://www.iris-biotech.de/). Theoretically, if a monolayer of PEG covering the AuNPs was present, the hydrodynamic diameter of these modified nanoparticles would be about 20 nm (assuming a linear molecule, *i.e.* "stretched"). However, the hydrodynamic diameter of AuNPs@PEG may be misrepresented. PEG is very flexible and may influence the Brownian motion of the particles by reducing the AuNPs dynamic viscosity and thus increasing their hydrodynamic diameter (Rahme et al. 2013).

### 3.2 AuNPs@PEG FUNCTIONALISED WITH SERUM ALBUMIN AND THE METALLIC COMPOUNDS

Serum albumin is the most abundant protein in blood plasma (Housni et al. 2008). This protein provides the intracellular binding, transportation and delivery of endogenous and exogenous compounds (Sankareswari et al. 2014, Trnková et al. 2010), such as fatty acids, steroids, metal ions, metabolites and a large number of pharmaceutical agents (Sankareswari et al. 2014). It is well known this ability of serum albumin to bind non-covalently with small molecules (Housni et al. 2008), resulting in an increased solubility of ligands in plasma and enhanced delivery to the

target sites (Can et al. 2012). Therefore, BSA and HSA have a great importance in nanomedicine due to their biocompatible, and also due to their water solubility. Their functionalisation with different functional groups on their surface also makes them an interesting targeted-based drug delivery system (Housni et al. 2008).

BSA is a globular protein composed of 583 amino acid residues. It contains three homologous domains (I – III), where each one comprises two sub-domains (A and B) paired by 17 disulfide bonds (Tayeh et al. 2009, Xu et al. 2013).The BSA binding sites for endogenous and exogenous molecules may be situated in sub-domains IIA and IIIA (Sudlow's sites I and II, respectively) (Xu et al. 2013). In the current work, the BSA was covalently bound to the synthesised AuNPs@PEG by using the EDC/sulfo-NHS reaction. The resulting AuNPs@PEG@BSA were then characterised by UV-Vis spectroscopy and DLS, and the number of BSA molecules per AuNP was estimated by the quantification of supernatants using the Bradford assay. The UV-Vis spectrum of AuNPs@PEG@BSA clearly shows a shift from 522 to 525 nm (see black line in Figure III.5), which is attributed to changes in the nature surrounding AuNPs@PEG due to BSA binding. The protein binding to PEG molecules was also confirmed through the DLS technique, where there was an increase in hydrodynamic diameter of the functionalised particles from 35.20 nm to 42.03 ± 0.75 nm. A final AuNP:BSA ratio of 1:5 (±1) was obtained by the Bradford assay (Figure VI.2, appendices). Considering a hydrodynamic diameter of 7 nm (Yohannes et al. 2010), and assuming a spherical conformation for the protein, the superficial area of each BSA is 153.86 $nm^2$. However, take into consideration the superficial area of an AuNP@PEG and the AuNP:BSA ratio, each BSA molecule was occupying 772.91 $nm^2$ in the particle. The coupling of proteins to the activated carboxyl groups carried out usually via lysines residues (Fischer 2010). Each BSA molecule has 60 lysines residues able to bind the activated carboxyl groups of PEG molecules (www.uniprot.org), which can lead to conformational changes of the protein, thus justifying the occupation of a larger area on the AuNP@PEG surface.

HSA shows 80 % similarity to BSA in primary structure (Sankareswari et al. 2014). HSA is composed of 585 amino acid residues, containing also 17 disulfide bonds and one free cysteine. Similar to the tertiary structure of BSA, HSA contains three homologous domains (I - III) which are divided into two sub-domains (A and B) (Can et al. 2012). AuNPs@PEG were also successfully functionalised with HSA. The UV-Vis spectrum shows a shift from 522 to 526 nm, confirming the protein binding to PEG molecules on the AuNP surface (see black line, Figure III.6). The increase in hydrodynamic diameter of HSA from 35 to 40.66 ± 0.70 nm, obtained by DLS technique, was consistent with the UV-Vis results. Bradford assay (Figure VI.3, appendices) corroborated that the amount of HSA coupled to AuNP@PEG was twice the amount of BSA, with the ratio 1:11 (±1) of AuNP:HSA . Despite being very similar proteins, HSA occupied a smaller area (353.05 $nm^2$/HSA) of the functionalised nanoparticle than BSA. Small changes in the amino acid sequences can have tremendous effects on protein structure. Many of the albumin differences are at residues that are surface-exposed and this is

reflected in terms of hydrophilicity/hydrophobicity of the HSA and BSA (Akdogan et al. 2012). The water molecules lead to their different conformational adaptability and flexibility, and BSA showed to be less flexible in a water solution than HSA, and in turn, HSA showed to be more hydrophobic than BSA (Akdogan et al. 2012). This reported study could explain the fact of having more HSA molecules on the surface of the functionalised particles than BSA molecules.

After protein functionalisation, AuNPs@PEG@BSA and AuNPs@PEG@HSA were incubated with TS262 and TS265 and characterised by UV-Vis spectroscopy, DLS and ICP-MS. A shift for longer wavelengths was observed when the metallic compounds binds to AuNPs@PEG@BSA than AuNPs@PEG@HSA. The bonding is corroborated by the DLS and ICP-MS results, showing, respectively, an increase in hydrodynamic diameters of the particles and higher compound:albumin ratios in almost all red-shifted samples.

The UV-Vis spectrum of AuNPs@PEG@BSA-TS262 shows a clearly shift from 525 to 533 nm (see red line, Figure III.5) and DLS showed a large increase in hydrodynamic diameter from 42.03 to 83.01 ± 1.43 nm. In turn, the UV-Vis spectrum of AuNPs@PEG@BSA-TS265 shows a shift from 525 to 535 nm (see blue line, Figure III.5) and DLS a large increase in hydrodynamic diameter from 42.03 to 88.60 ± 5.80 nm. The amount of TS262 and TS265 molecules per AuNP@PEG@BSA, after digestion with *aqua regia,* was determined by ICP-MS technique to be 764 ± 120 and 612 ± 23 molecules, respectively. According to the results obtained by UV-Vis and DLS, it was expected that the amount of TS265 molecules per AuNP@PEG@BSA was higher than TS262 molecules. Nevertheless, AuNPs@PEG@BSA can have a greater number of TS265 on their surface, since the SEM associated to the number of TS262 molecules was quite large, and the result could be unreliable. Several samples with different concentrations of functionalised particles and compounds were analysed by ICP-MS, and with different incubation times (data not shown). The higher ratios of compound:AuNP were observed in all the conditions used in this work.

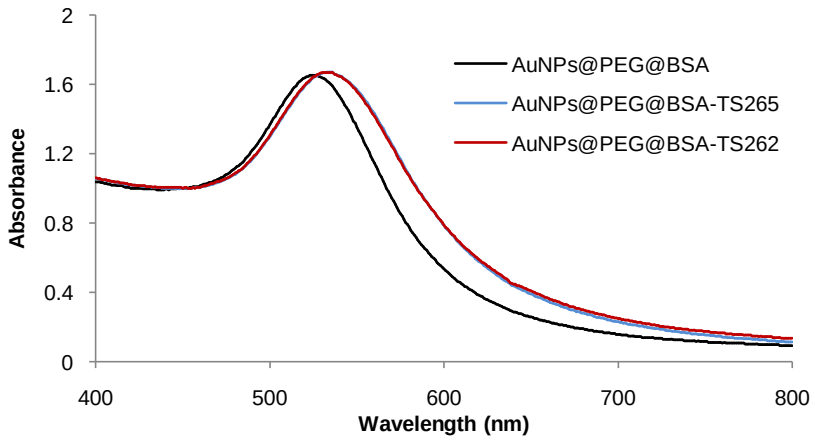


Figure III.5 – Spectra corresponding to the AuNPs@PEG@BSA, AuNPs@PEG@BSA-TS262, AuNPs@PEG@BSA-TS265, obtained by UV-Vis spectroscopy in the wavelength range of 400 - 800 nm (pH 7.0).

Regarding the AuNPs@PEG@HSA-TS262, the UV-Vis spectrum shows a shift from 526 to 529 nm (see red line, Figure III.6) and an increase in hydrodynamic diameter from 40.66 to 76.21 ± 1.55 nm was observed by DLS. Regarding the AuNPs@PEG@HSA-TS265, the UV-Vis spectrum also shows a shift for higher wavelengths from 526 to 532 nm (see blue line, Figure III.6), and the DLS results are in agreement with these obtained data, confirming the successful link of the compound to the functionalised nanoparticles, with an increase in hydrodynamic diameter from 40.66 to 84.67 ± 1.68 nm. The amount of TS262 and TS265 molecules per AuNPs@PEG@HSA was also determined by ICP-MS in 307 ± 23 and 432 ± 8 molecules, respectively.

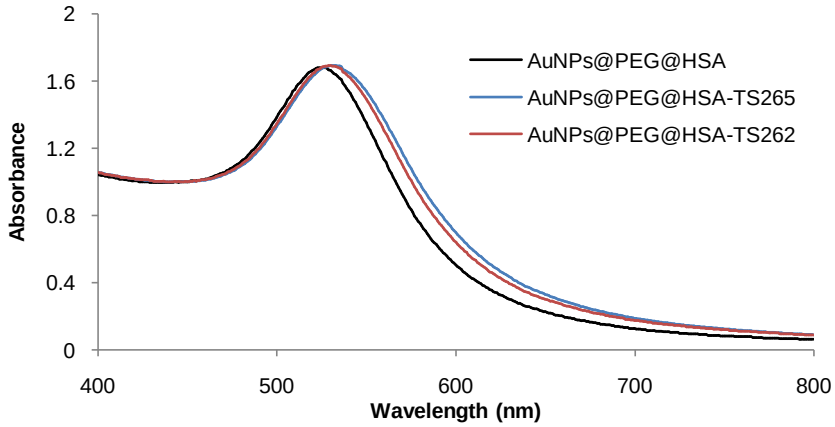


Figure III.6 – Spectra corresponding to the AuNPs@PEG@HSA, AuNPs@PEG@HSA-TS262, AuNPs@PEG@HSA-TS265, obtained by UV-Vis spectroscopy in the wavelength range of 400 - 800 nm (pH 7.0).

According to these results, the ability of BSA to bind the metallic compounds was higher than that of HSA. Despite the lower amount of BSA on the particle compared to the amount of HSA (5 vs. 11 proteins per AuNP, respectively) there was an increase in the final concentrations of both compounds bound to BSA. For both cases this shows that a significant number of molecules may carried on these developed AuNPs drug delivery vehicles.

Presence of the compounds on the AuNPs' surface was also demonstrated via the alterations of the maximum absorbance wavelengths of TS262 and TS265 (254 nm and 253 nm for TS262 and TS265, respectively) (Figure VI.4, appendices) The UV-Vis spectra corresponding to the functionalised AuNPs clearly show the presence of both compounds surrounding AuNPs@PEG@BSA and AuNPs@PEG@HSA (Figure VI.5 and Figure VI.6, appendices). The molar extinction coefficients was determined: 55300 $M^{-1}$ $cm^{-1}$ and 34900 $M^{-1}$ $cm^{-1}$ for TS262 and TS265, respectively (Figure VI.7 and Figure VI.8, appendices).

Although many studies based on serum albumin-AuNPs nanosystems have been described, most of them are performed with BSA and only a small number are reported with the albumin from the human serum. The current work provides the advantage of develop a HSA-AuNP

bioconjugate for drug delivery and also the opportunity of compare it with the homologous BSA-AuNP nanosystem.

## 4. CYTOTOXICITY ASSAYS OF FUNCTIONALISED AuNPs

After obtaining the functionalised and characterised AuNPs, *in vitro* cytotoxicity assays in HCT116, A549 and H1975 cell lines were performed. For that, cell viability assays for functionalised AuNPs (taking into consideration the compounds at their relative $IC_{50}$) were made. We intended to verify if the functionalised AuNPs carrying the compounds could bring advantages compared to the use of free TS262 and TS265 in cancer treatment (*e.g.* dose reduction, reduced toxicity in healthy cells, etc).

The cells were exposed to the functionalised AuNPs for 48 hours and the evaluation of the induced cytotoxicity was performed by MTS assay. Figure III.7 shows the percentage of cell viability obtained for the A549 cell line. AuNPs@PEG@BSA and AuNPs@PEG@HSA decreased the cell viability of about 30 % and 40 %, respectively. In turn, those functionalised AuNPs carrying the TS265 reduced the cell viability in approximately 80 %. It should be noted that this decrease of cell viability was attained at the concentration of free TS265 that induced 50 % of cell death. Thus, the combined treatment resulted in a greater inhibition of cell activity than single treatment with TS265. The results suggested that there was an additive effect of AuNPs@PEG@BSA or AuNPs@PEG@HSA and TS265 since there was a significant negative effect in cell viability resulting from both systems. Hence, the developed AuNP-based nanosystems demonstrated to be efficient drug delivery systems for TS265 in A549 tumour cell line.

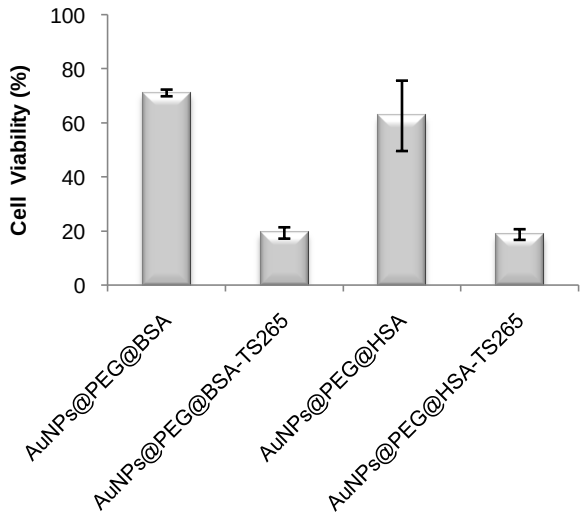


Figure III.7 – Cell viability in A549 human cell line obtained by MTS assay after exposure to functionalised AuNPs for 48 hours. In this assays was used the concentration of the functionalised AuNPs that contains the amount of TS265 corresponding to its previous determined relative $IC_{50}$ (see section III.1). The percentage of cell viability for each formulation is relative to the mean of two independent assays and error bars are correspondent to SEM.

In A549 cancer cell line and under the same incubation conditions (*i.e.* volume of solution used, dilution of the functionalised AuNPs in culture medium, etc) it was not possible to reach the corresponding relative $IC_{50}$ of TS262 on AuNPs@PEG@HSA surface. Thus, for this cell line only the AuNPs nanoconjugates containing the TS265 compound were used.

The AuNPs@PEG@BSA and AuNPs@PEG@HSA triggered a slight decrease (approximately 5 % and 10 %, respectively) in the viability of H1975 cancer cells (Figure III.8). This shows the nanoconjugates' low toxicity in this type of cancer cells. The AuNPs carrying the TS262 (Figure III.8A) demonstrated to have a less pronounced anti-proliferative potential than the AuNPs containing TS265 on their surface (Figure III.8B).

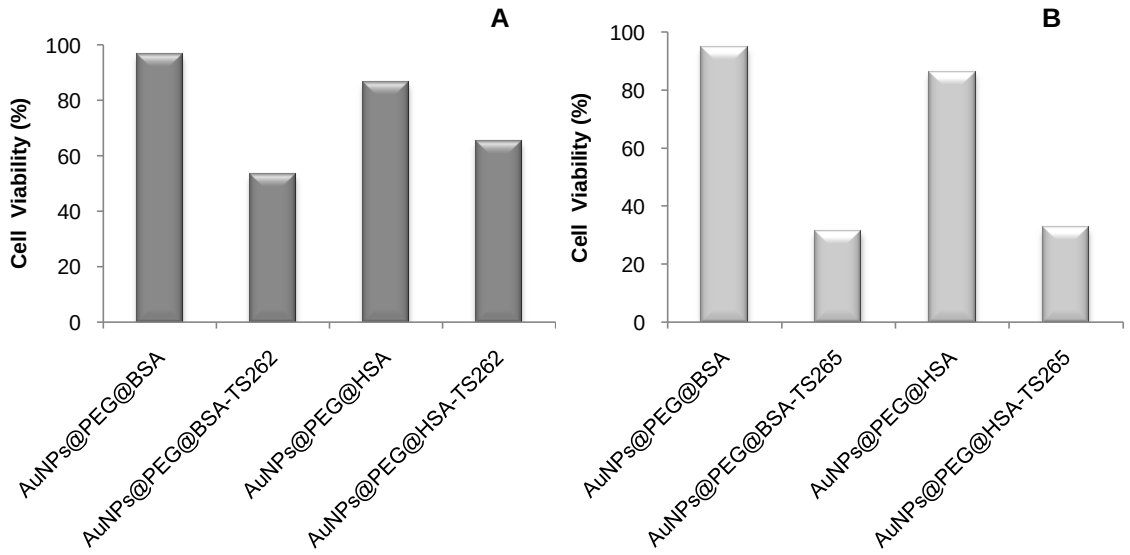


Figure III.8 – Cell viability in H1975 human cell line obtained by MTS assay after exposure to functionalised AuNPs for 48 hours: (A) functionalised AuNPs with and without TS262 and (B) functionalised AuNPs with and without TS265. In this assays was used the concentration of the functionalised AuNPs that contains the amount of TS262 or TS265 corresponding to its previous determined relative $IC_{50}$ (see section III.1). The percentage of cell viability for each formulation is relative to one assay.

The reduction on cell viability obtained for AuNPs@PEG@BSA-TS262 and AuNPs@PEG@HSA-TS262 was about 50 % and 40 %, respectively, indicating the similarity with the use of the TS262 alone to induce cell death in H1975 cancer cells. Thus, in regard to a possible reduction of the required dose of this anticancer agent, there was no advantage of using those nanoparticle systems in this type of lung cancer.

Both AuNPs@PEG@BSA-TS265 and AuNPs@PEG@HSA-TS265 demonstrated to be promising targeted-based drug delivery systems. There was a pronounced decrease in H1975 cell viability of about 70 % in both cases, at the TS265 concentration that induced 50 % of cell death when the compound was used in the free form. These results suggested that there was a synergistic effect of AuNPs@PEG@BSA or AuNPs@PEG@HSA and TS265 since the TS265 anticancer effect was enhanced when combined with the functionalised AuNPs.

Absence of cytotoxicity from AuNPs@PEG@BSA and AuNPs@PEG@HSA in HCT116 cell line is shown in Figure III.9.

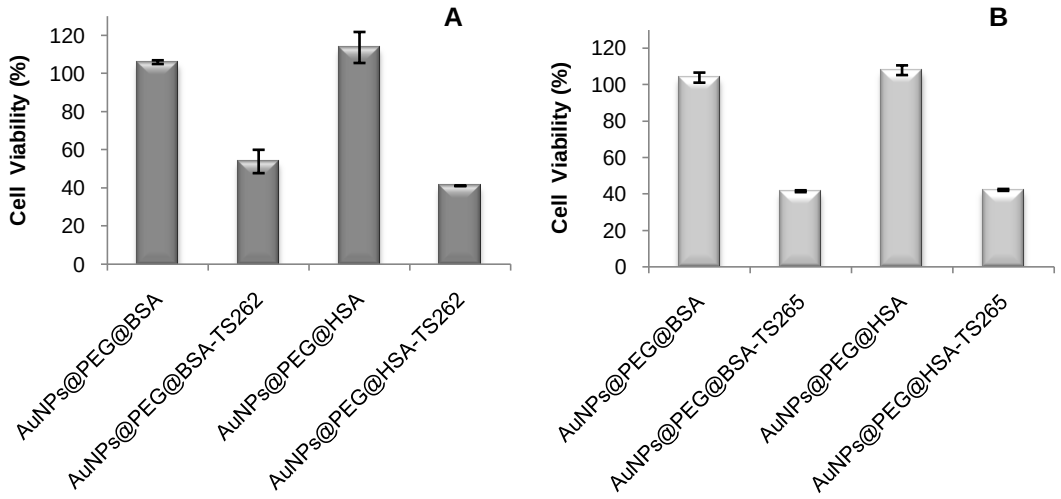


Figure III.9 – Cell viability in HCT116 human cell line obtained by MTS assay after exposure to functionalised AuNPs for 48 hours: (A) functionalised AuNPs with and without TS262 and (B) functionalised AuNPs with and without TS265. In this assays was used the concentration of the functionalised AuNPs that contains the amount of TS262 or TS265 corresponding to its previous determined relative $IC_{50}$ (Silva et al. 2013b). The percentage of cell viability for each formulation is relative to the mean of two independent assays and error bars are correspondent to SEM.

The HCT116 cancer cells exposed to AuNPs@PEG@BSA-TS262 and AuNPs@PEG@HSA-TS262 suffered a reduction in cell viability of approximately 50 % and 60 %, respectively. The AuNPs@PEG@BSA-TS262 system showed an equivalent anti-proliferative potential to that of TS262 alone. Hence, for H1975 cancer cells, the proposed nanoconjugate brings no benefit in terms of reducing the required dose to induce a substantial effect. However, exposure the HCT116 cancer cells to AuNPs@PEG@HSA and AuNPs@PEG@HSA-TS262 systems, suggest a synergistic effect of AuNPs@PEG@HSA and TS262, since the TS262 anti-proliferative potential was enhanced in 10 % when combined with the functionalised AuNPs.

It was also observed that either AuNPs@PEG@BSA-TS265 or AuNPs@PEG@HSA-TS265 had an inhibitory effect of about 60 % on HCT116 cellular activity. Thus, the treatment with a combination of functionalised AuNPs and TS265 decreased the cell viability in more 10 % compared to the use of TS265 alone. Since the functionalised particles without the compound on their surface showed no toxicity in HCT116 cancer cells and the effect of TS265 was enhanced, it also suggests that AuNPs@PEG@BSA or AuNPs@PEG@HSA work synergistically with TS265 to reduce the viability of HCT116 cancer cells.

Briefly, the results suggested that AuNPs@PEG@BSA-TS265 and AuNPs@PEG@HSA-TS265 may provide promising alternative systems for cancer treatment, being able to reduce *in vitro*

the required doses of the TS265 in A549, H1975 and HCT116 cell lines. Also the AuNPs@PEG@HSA-TS262 showed to be a favourable *in vitro* drug delivery system, reducing the required doses of TS262 in HCT116 cell line. Only the AuNPs@PEG@BSA-TS262 showed no advantage comparing to the anti-proliferative effect of the compound alone in the two tested cell lines.

## 5. STEADY-STATE FLUORESCENCE – INTERACTION OF TS262 AND TS265 WITH SERUM ALBUMIN

The tertiary structure and function of proteins are shaped by electrostatic interactions that it maintains with its surrounding environment. Fluorescence from the tryptophan appeared as an easily method for probing electrostatic interactions since this amino acid is highly sensitive to the polarity of the environment (Vivian & Callis 2001). Therefore, the intrinsic fluorescence of tryptophan is commonly used to monitor conformational changes in the proteins due to protein-ligand interactions (Shi et al. 2012). The maximum emission wavelength of tryptophan is correlated with the degree of exposure to the surrounding solvent, ranging from ~308 to ~355 nm (Vivian & Callis 2001). Besides tryptophan, tyrosine and phenylalanine are two other amino acid residues that contribute to the UV fluorescence of the proteins. However, when protein fluorescence is excited at wavelengths equal or longer than 295 nm, the absorption is due mainly to tryptophan (Lakowicz 2006).

Each BSA molecule has two tryptophan residues, Trp-134 and Trp-212, located near the surface of the molecule in sub-domain IB (hydrophilic environment) and in a hydrophobic pocket in sub-domain IIA, respectively (Trnková et al. 2010). HSA has one single tryptophan residue, Trp-214, contributing to its intrinsic fluorescence, and is located in a similar hydrophobic environment (sub-domain IIA) than Trp-212 of BSA (Kamal & Behere 2005). Taking advantage of the intrinsic fluorescence of BSA and HSA due to its tryptophan residues, the fluorescence quenching of these proteins at various concentrations of TS262 and TS265 were studied. The great purpose of these assays was to confirm that each BSA and HSA molecules could interact with the number of TS262 and TS265 molecules determined by ICP-MS. For that, was fixed a concentration of 2.0 µM for each serum albumin, varying the compound concentrations, in which was tested the compound concentration corresponding to the ratio compound:AuNP obtained by ICP-MS technique, and further concentrations above and below this.

The fluorescence quenching spectra of BSA at different concentrations of TS262 is shown in Figure III.10. In the absence of TS262, the maximum emission wavelength was attributed only to the intrinsic fluorescence of BSA molecule and was observed at 350 nm (see “free BSA” in Figure III.10 and Figure III.11). The effect of TS262 complex on BSA molecule was very pronounced, in which there was a remarkable intrinsic fluorescence decrease of BSA with the increase of compound concentration, reaching a decrease of about 89 % at the highest TS262 concentration used (*i.e.* 400 µM) – see *inset* in Figure III.10.

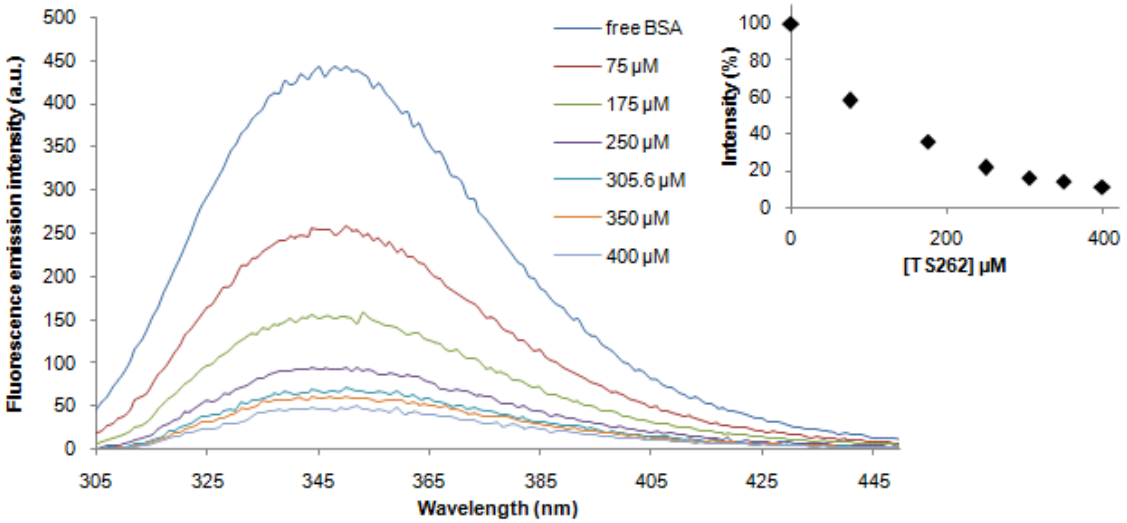


Figure III.10 – Steady-state fluorescence quenching spectra of BSA (fixed concentration at 2.0 µM) obtained through the binding of increasing concentrations of TS262 complex (0 – 400 µM), incubated for 1 hour at 4ºC in 10 mM pH 7 phosphate buffer/0.15 M NaCl ($\lambda_{exc}$ = 295 nm). The tested concentration of 305.6 µM of TS262 was equivalent to the molar ratio of TS262:AuNP@PEG@BSA, obtained by ICP-MS. *Inset*: percentage of relative fluorescence intensity of BSA at $\lambda_{em}$ = 350 nm with increasing complex concentration.

The steady-state fluorescence spectra of BSA incubated with TS265 (Figure III.11) shows that the BSA fluorescence emission intensity decreased as well with the increase of TS265 concentrations. In this case there was a decay of about 91 % of the intrinsic fluorescence of BSA at the highest TS265 concentration used (*i.e.* 375 µM) – see *inset* in Figure III.11.

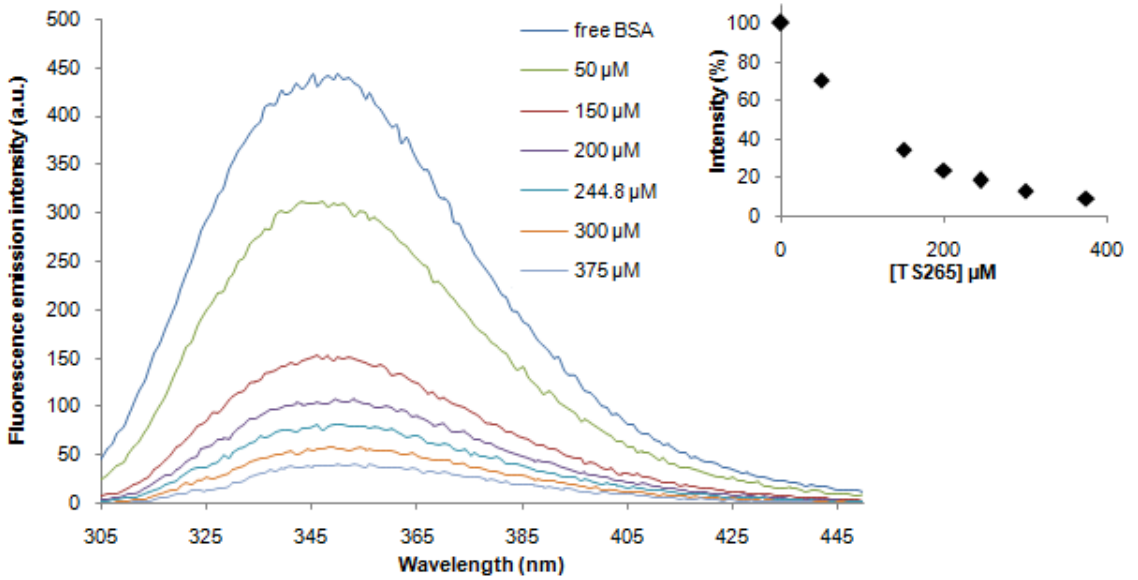


Figure III.11 – Steady-state fluorescence quenching spectra of BSA (fixed concentration at 2.0 µM) obtained through the binding of increasing concentrations of TS265 complex (0 – 375 µM), incubated for 1 hour at 4ºC in 10 mM pH 7 phosphate buffer/0.15 M NaCl ($\lambda_{exc}$ = 295 nm). The tested concentration of

244.8 µM of TS265 was equivalent to the molar ratio of TS265:AuNP@PEG@BSA, obtained by ICP-MS. *Inset*: percentage of relative fluorescence intensity of BSA at $\lambda_{em}$ = 350 nm with increasing complex concentration.

As the fluorescence intensity of BSA gradually decreased when the concentrations of TS262 or TS265 increased, it was confirmed that the compounds act as quenchers and exists the interaction between them and the fluorophore. It is described that the ability of albumin to associate non-covalently with smaller molecules and ions is due to the existence of at least six binding regions in the protein, two high affinity binding sites, situated in Sudlow's sites I and II as previously described, and a number of sites with lower affinity for ligands (Shahabadi et al. 2012). In these fluorescence studies, the BSA was in its native conformation, in the absence of the compounds, contrary to the BSA molecules covalently linked to PEG on the AuNPs surface. The as-prepared AuNPs@PEG@BSA was incubated with a high concentration of compounds (50 µM), and was verified by ICP-MS technique that the maximum of molecules that the protein could bind was about 153 and 122 molecules of TS262 and TS265, respectively (764 ± 120 and 612 ± 23 molecules of TS262 and TS265 per AuNP, respectively, as previously described in section III.3.2). When were tested higher molar ratios of compound:BSA than these, and analysed by steady-state fluorescence, it was confirmed that each BSA molecule could interact with a great number of TS262 and TS265 molecules since there was still a decay in fluorescence, which was an evidence for continuous conformational changes of BSA. The fact of BSA be covalently bound to PEG in AuNPs@PEG@BSA may lead to the steric hindrance of the molecule due to its altered tertiary structure, and also lead to the occupation of several binding sites, interacting with less molecules than in its free conformation. The fact that they are only described two high affinity sites for the binding of ligands to BSA, suggests that almost all TS262 and TS265 molecules were bound to a large number of weaker binding sites. The interactions of TS262 and TS265 with these lower affinity sites for ligands could be also supported by the fact of the quenching of the tryptophan residues fluorescence was very strong at lower molar ratios, but in higher molar ratios it progressed weakly, suggesting weaker binding sites for the compounds, and probably located away from the fluorophore. The nature of the interaction between almost all compound molecules and BSA could be electrostatic since the isoelectric point of BSA is 4.7 (Chaudhary et al. 2014) and the experimental pH ~7, *i.e.* BSA possesses a negative charge whereas the compounds are positive charged.

Incubated at the same conditions, the maximum emission wavelength of free HSA (*i.e.* in the absence of TS262 or TS265) was observed at 344 nm (see "free HSA" in Figure III.12 and Figure III.13) instead of a maximum wavelength of 350 nm, attributed to the fluorescence intensity of free BSA. The difference between the maximum emission wavelengths of free BSA and free HSA can be related with the presence of Trp-134 in BSA, which is located in a more hydrophilic environment than the Trp-212 or the Trp-214 in HSA, influencing the maximum emission for longer wavelengths by being more exposed to the solvent (Varlan & Hillebrand 2010). Furthermore, the maximum intensity of the fluorescence emission of BSA was

approximately twice than the maximum intensity of HSA in the absence of the compounds, suggesting that the Trp-134 has similar fluorescence intensity than Trp-212 and Trp-214.

The gradual decay of the intrinsic fluorescence of HSA was also observed as the concentration of TS262 increased (Figure III.12). There was an effect of the TS262 complex on HSA molecule which leads to a decrease in fluorescence of about 65 % at the higher molar ratio tested (*i.e.* 90 µM) – see *inset* in Figure III.12.

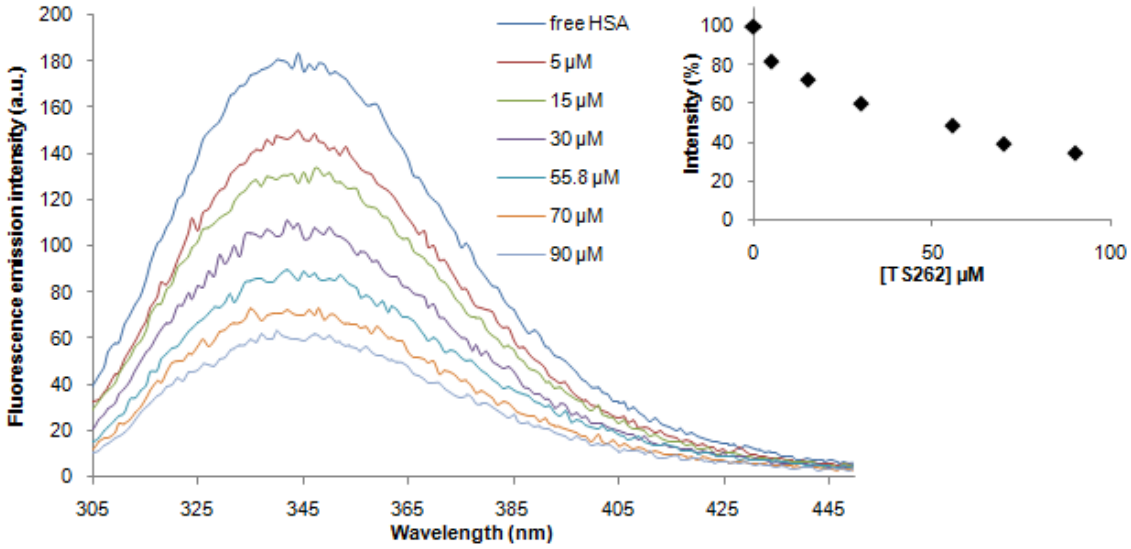


Figure III.12 – Steady-state fluorescence quenching spectra of HSA (fixed concentration at 2.0 µM) obtained through the binding of increasing concentrations of TS262 complex (0 – 90 µM), incubated for 1 hour at 4ºC in 10 mM pH 7 phosphate buffer/0.15 M NaCl ($\lambda_{exc}$ = 295 nm). The tested concentration of 55.8 µM of TS262 was equivalent to the molar ratio of TS262:AuNP@PEG@HSA, obtained by ICP-MS. *Inset*: percentage of relative fluorescence intensity of HSA at $\lambda_{em}$ = 344 nm with increasing complex concentration.

The steady-state fluorescence spectra of HSA incubated at different concentrations of TS265 also shows a reduction in fluorescence emission intensity with the increasing of the compound concentration (Figure III.13). In this case there was a decay of about 82 % of the intrinsic fluorescence of free HSA at the highest TS265 concentration tested (*i.e.* 130 µM) – see *inset* in Figure III.13. The data corresponding to the incubation of the protein with a final concentration of 10 µM of TS265 does not make sense. The fluorescence intensity was not in agreement with the results obtained at higher molar ratios of TS265:HSA (*i.e.* equal or higher than 30 µM of TS265) - see *inset* in Figure III.13. An error may have occurred while preparing the solution and the data should be excluded.

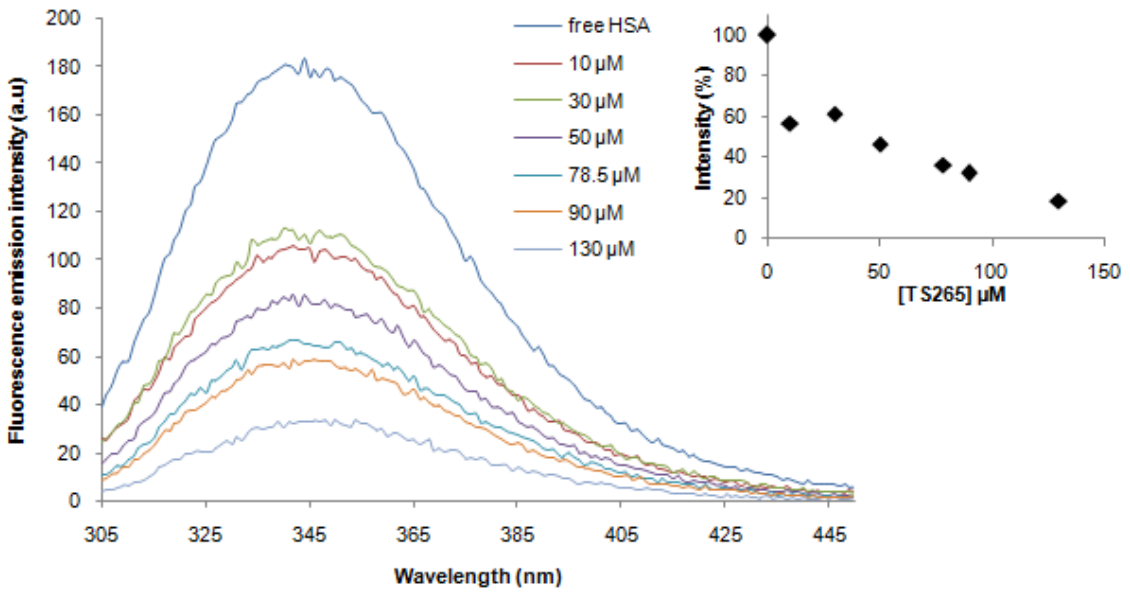


Figure III.13 – Steady-state fluorescence quenching spectra of HSA (fixed concentration at 2.0 µM) obtained through the binding of increasing concentrations of TS265 complex (0 – 130 µM), incubated for 1 hour at 4ºC in 10 mM pH 7 phosphate buffer/0.15 M NaCl ($\lambda_{exc}$ = 295 nm). The tested concentration of 78.5 µM of TS265 was equivalent to the molar ratio of TS265:AuNP@PEG@HSA, obtained by ICP-MS. *Inset*: percentage of relative fluorescence intensity of HSA at $\lambda_{em}$ = 344 nm with increasing complex concentration.

The results obtained by the steady-state fluorescence assays for the binding of HSA to TS262 or TS265 molecules also confirmed the interaction between the protein and both compounds. Several binding sites have been reported for HSA. Nevertheless it is accepted the dominance of two high affinity sites for the binding of ligands, situated at Sudlow's sites I and II (Can et al. 2012), such as in the homologous BSA. As well as BSA, it was confirmed in these assays that the HSA could interact with a large number of TS262 or TS265 molecules when the protein was in its native conformation compared to HSA covalently bounded to PEG in AuNPs@PEG@HSA. The AuNPs@PEG@HSA was also incubated with a high concentration of compounds (50 µM), and was verified by ICP-MS technique that the maximum of molecules that the protein could bind was about 28 and 39 molecules of TS262 and TS265, respectively (307 ± 23 and 432 ± 8 molecules of TS262 and TS265 per AuNP, respectively, as previously described in section III.3.2). Higher molar ratios of compound:HSA still show a decay in fluorescence emission, being an evidence of continuous interactions between TS262 or TS265 and the possible binding sites of HSA. In fact, the existence of one binding site for TS265 at a distance of ~1.5 nm from Trp-214 has been reported, not excluding other binding sites for the ligand (Luís et al. 2014). This study also reported the existence of a reversible interaction of the compound with the HSA, indicating its promising potential to be delivery in tumour cells, taking advantage of the passive targeting (Luís et al. 2014). Since there are only two reported high affinity sites for ligands, it is supposed that a great amount of those TS262 and TS265 molecules bind to the lower affinity sites of HSA. The isoelectric point of HSA is 4.7 at the

experimental pH (pH 7) (Vlasova & Saletsky 2009), which would reflect in a negative charge that could interact with the positive charge of the compounds.

As the fluorescence quenching refers to excited-state reactions, molecular rearrangements, energy transfer, ground-state complex formation or collisional quenching (Varlan & Hillebrand 2010), complementary studies are needed to understand the nature of the quenching induced by TS262 and TS265 on the BSA and HSA fluorescence. It would be also interesting to develop these fluorescence studies in order to obtain the binding affinity constants of the compounds to BSA and HSA.

## IV. CONCLUSIONS AND FUTURE PERSPECTIVES

The success of chemotherapy in cancer treatment is dependent on the development of such platforms capable of carry and delivers the chemotherapeutics in the desired cells, lessening the impact of toxic side effects on healthy cells. Bionanotechnology offers a wide range of innovations regarding drug delivery nanosystems to be used in medicine, which result in increased drug concentrations inside cancer cells, allowing higher doses compared with free drug. The present work describes the development of AuNPs-based systems – AuNPs@PEG@BSA and AuNPs@PEG@HSA - for carrying two metallic compounds with anti-proliferative potential, TS262 and TS265, in HCT116, A549 and H1975 cancer cell lines.

In the current work it was verified the similarity in the TS262 and TS265 cytotoxicity within the same cancer cell line, in which the relative $IC_{50}$ was determined in 0.714 ± 0.091 μM and 0.741 ± 0.007 μM in A549 cell line, and 0.355 ± 0.038 μM and 0.349 ± 0.021 μM in H1975 cell line, for TS262 and TS265 respectively. The anti-proliferative effect of TS265 in MCF-10A has been reported as null at concentrations smaller than 1 μM. This is a positive result considering the relative $IC_{50}$ for the TS265 compound in the three tested epithelia type cancer cell lines.

A monodisperse solution of spherical AuNPs were successfully synthesised with a mean diameter of about 14 nm (14.26 ± 0.31 nm obtained by TEM and a mean hydrodynamic diameter of 14.14 ± 0.43 nm obtained by DLS) and a maximum and symmetric absorption peak observed at 519 nm. These particles were then functionalised, in which were obtained four different systems for drug delivery in cancer cells - AuNPs@PEG@BSA-TS262, AuNPs@PEG@BSA-TS265, AuNPs@PEG@HSA-TS262 and AuNPs@PEG@HSA-TS265 – with the maximum absorption peaks observed by UV-Vis at 533 nm, 535 nm, 529 nm and 532 nm, and a mean hydrodynamic diameters obtained by DLS of 83.01 ± 1.43 nm, 88.60 ± 5.80 nm, 76.21 ± 1.55 nm and 84.67 ± 1.68 nm, respectively. The cellular uptake of the functionalised AuNPs was confirmed by the cytotoxicity assays results in HCT116, A549 and H1975 cancer cell lines, and it was observed that the cellular response to AuNPs was dependent on the tested cancer cells type. Specifically, the nanosystems containing the TS265 compound - AuNPs@PEG@BSA-TS265 and AuNPs@PEG@HSA-TS265 – showed the ability to reduce *in vitro* the required doses of the TS265 in HCT116, A549 and H1975 cancer cells. The AuNPs@PEG@HSA-TS262, tested under the same conditions, also showed to be a promising *in vitro* drug delivery system, able to reduce the required doses of TS262 in HCT116 cancer cell line. The AuNPs@PEG@BSA-TS262 do not shown any advantage compared to TS262 administered alone in the HCT116 and H1975 cancer cell lines.

ICP-MS allowed to calculate the amount of TS262 and TS265 molecules bound per AuNP@PEG@BSA (764 ± 120 and 612 ± 23 molecules, respectively) and per AuNP@PEG@HSA (307 ± 23 and 432 ± 8 molecules, respectively). The fluorescence assays were in agreement with these results, showing the interaction between the serum proteins, in its free form, and the compounds, at higher molar ratios compared to the ICP-MS results.

All pre-defined objectives for this thesis have been accomplished but there are still many milestones that can be further developed in the future:

i) The anti-proliferative effect of free TS262 in MCF-10A healthy epithelial cells from mammary gland should be addressed;

ii) It is important to pursue the studies trying to prove the potential of these nanosystems by decreasing the side toxic effects of chemotherapy, affecting less the healthy cells. In this regard, the AuNPs functionalised with the TS262 can bring advantages compared to the use of free drug in cancer treatment. For that, *in vitro* cytotoxicity assays in healthy cells (*e.g.* MCF-10A) should be performed, and if no toxicity from the functionalised AuNPs is verified, *in vivo* assays should be also carried out. The *in vivo* studies will allow knowing, beyond biocompatibility, if there is any AuNPs accumulation in organs which are not targeted, and also the blood circulation time of the particles. Non-targeted nanoparticles have been reported to significantly improve drug bioavailability and the high accumulation of anticancer agents in cancer cells due to EPR effect;

iii) Understanding the mechanisms of AuNPs internalisation into cells is important for the drug delivery. Their internalisation is dependent on surface coating and AuNP size. Internalisation of AuNPs could be tracked, possible via transmission electron microscopy or fluorescent optical microscopy in order to study the mechanism of internalisation in living cells;

iv) Adapting the developed nanosystems for active targeting and study the possible advantages compared to the passive targeting. Several molecular targeted agents have been studied for this purpose in order to obtain personalised therapies for each type of cancer. The epidermal growth factor receptor (EGFR) is a transmembrane tyrosine kinase receptor that is abnormally amplified and/or activated in a variety of cancers (Perez-Torres et al. 2006). More than 60 % of non-small cell lung carcinomas overexpress EGFR, making anti-EGFR therapies very attractive for the treatment of these cancer types (Santos et al. 2011). Tyrosine kinase inhibitors for EGFR, such as Erlotinib and Afatinib (American Cancer Society, 2014), and monoclonal antibodies against the extracellular domain of EGFR, *e.g.* Cetuximab have demonstrated an anti-proliferative effect on cancer cells (Doody et al. 2007, Hsu et al. 2010). A monoclonal antibody to vascular endothelial growth factor (VEGF), Bevacizumab, has been also used in targeted therapies for non-small cell lung cancers (American Cancer Society, 2014). The developed AuNPs can be functionalised in the future with any of these referenced agents for targeted therapies in lung cancers. In turn, the two most important targeted drugs in colorectal cancer include VEGF, a protein that regulates the process of angiogenesis, and EGFR pathways (Chee & Sinicrope, 2010). The anti-VEGF agents Bevacizumab and Ziv-aflibercept, and the anti-EGFR monoclonal antibodies Cetuximab and Panitumumab, are approved for the treatment of

colorectal cancer (American Cancer Society, 2013). As well as in non-small cell lung cancers, the EGFR are up-regulated in more than 60 % of colorectal cancer cases (Chee & Sinicrope, 2010), being an important target for the development of new therapies for colorectal cancer. Thus, either the referenced anti-VEGF or anti-EGFR agents can be used to functionalise the developed AuNPs for active targeting-based therapy in colorectal cancer;

v) Complementary fluorescence studies are needed to understand the nature of the observed quenching of BSA and HSA due to the presence of the compounds, and it would be also interesting to develop these fluorescence studies in order to obtain the binding affinity constants of the TS262 to HSA and BSA, and the binding affinity constant of the TS265 to BSA.

Although a wide range of nanomaterials have been used for cancer treatment, the bionanotechnology remains in early stages, and the safety of such materials in nanomedicine needs to be fully understood. However it is believed that the development of targeted and non-targeted nanosystems for drug delivery will bring a significant increase in the cure of several types of cancer in which treatments are not completely effective, or cancers do not have cures today. It is noteworthy that the four developed AuNPs-based nanosystems for drug delivery can be applied in nanomedicine, in principle, to a plethora of other cancer types.

## V. REFERENCES


Abdelhalim MAK, Mady MM, Ghannam MM. 2011. Rheological and dielectric properties of different gold nanoparticle sizes. *Lipids Health Dis.* 10(208):10 pages.

Alexis F, Pridgen EM, Langer R, Farokhzad OC. 2010. Nanoparticle techonologies for cancer therapy. In *Handbook of Experimental Pharmacology*, ed M Schäfer-Korting. 197:55–86. Berlin, Heidelberg: Springer Berlin Heidelberg

Akdogan Y, Reichenwallner J, Hinderberger D. 2012. Evidence for water-tuned structural differences in proteins: an approach emphasizing variations in local hydrophilicity. *Plos one.* 7(9): 11 pages.

Anand P, Kunnumakkara AB, Sundaram C, Harikumar KB, Tharakan ST, et al. 2008. Cancer is a preventable disease that requires major lifestyle changes. *Pharm. Res.* 25(9):2097–2116

Atkins P w., Overton TL, Rourke JP, Weller MT, Armstrong FA. 2010. An introduction to coordination compounds. In *Inorganic chemistry*, pp. 199–222.

Baptista P, Doria G, Henriques D, Pereira E, Franco R. 2005. Colorimetric detection of eukaryotic gene expression with dna-derivatized gold nanoparticles. *J. Biotechnol.* 119(2):111–17.

Baptista P, Pereira E, Eaton P, Doria G, Miranda A, et al. 2008. Gold nanoparticles for the development of clinical diagnosis methods. *Anal. Bioanal. Chem.* 391(3):943–50.

Bartczak D, Kanaras AG. 2011. Preparation of peptide-functionalized gold nanoparticles using one pot edc/sulfo-nhs coupling. *Langmuir*. 27:10119–23.

Bharti SK, Singh SK. 2009. Recent developments in the field of anticancer metallopharmaceuticals. . 1(4):1406–20.

Brown SD, Nativo P, Smith J-A, Stirling D, Edwards PR, et al. 2010. Gold nanoparticles for the improved anticancer drug delivery of the active component of oxaliplatin. *J. Am. Chem. Soc.* 132:4678–84.

Bruijnincx PCA, Sadler PJ. 2008. New trends for metal complexes with anticancer activity. *Curr Opin Chem Biol*. 12(2):197–206.

Cabral RM, Baptista P V. 2013. The chemistry and biology of gold nanoparticle-mediated photothermal therapy: promises and challenges. *Nano Life*. 3(3):18 pages.

Cai W, Gao T, Hong H, Sun J. 2008. Applications of gold nanoparticles in cancer nanotechnology. *Nanotechnol. Sci. Appl.* 1:17–32.

Can F, Maduen R, Sevilla JM, Bla M, Pineda T. 2012. Role of the functionalization of the gold nanoparticle surface on the formation of bioconjugates with human serum albumin

Cao W, Gu Y, Meineck M, Xu H. 2014. The combination of chemotherapy and radiotherapy towards more efficient drug delivery. *Chem. Asian J.* 9:48–57.

Chabner BA, Jr TGR. 2005. Chemotherapy and the war on cancer. *Nat. Rev. - Cancer*. 5:65–72

Chakraborty C, Pal S, Priya Doss G, Wen Z-H, Lin C-S. 2013. Nanoparticles as “smart” pharmaceutical delivery. *Forntiers Biosci.* 18:1030–50.

Chaudhary A, Gupta A, Khan S, Nandi CK. 2014. Morphological effect of gold nanoparticles on the adsorption of bovine serum albumin. *Phys. Chem. Chem. Phys.* 12 pages.

Chee CE, Sinicrope FA. 2010. Targeted therapeutic agents for colorectal cancer. *Gastroenterol Clin North Am*. 39(3):601-613.

Chow AY. 2010. Cell cycle control by oncogenes and tumor suppressors: driving the transformation of normal cells into cancerous cells. *Nat. Educ.* 3(9):7.

Cytimmune, The elements of Aurimune. http://www.cytimmune.com/ (accessed in May, 2014).

Conde J, Baptista P V, Hernandez Y, Sanz V, de la fuente JM. 2012a. Modification of plasmid dna topology by "histone-mimetic" gold nanoparticles. *nanomedicine*. 7(11):1657–66.

Conde J, Doria G, Fuente JM De, Baptista PV. 2012b. Rna quanti fi cation using noble metal nanoprobes: simultaneous identi fi cation of several different mrna targets using color multiplexing and application to cancer diagnostics. In *Nanoparticles in Biology and Medicine: Methods and Protocols*, ed M Soloviev. 906:71–87. Totowa, NJ: Humana Press.

Conde J, Tian F, Baptista P V, de la Fuente JM. 2014. Multifunctional gold nanocarriers for cancer theranostics – from bench to bedside and back again ? In *Nano-oncologicals: new targeting and delivery approaches,* ed Alonso MJ, Garcia-Fuentes M. Chapter 11, 49 pages.

Cooper GM. 2000. Cancer: the development and causes of cancer. In *The Cell: A Molecular Approach.*

Costello LC, Franklin RB. 2012. Cytotoxic/tumor suppressor role of zinc for the treatment of cancer: an enigma and an opportunity. *Expert rev Anticancer ther*. 12(1):121–28.

Curtin NJ. 2012. Dna repair dysregulation from cancer driver to therapeutic target. *Nat. Rev. - Cancer*. 12:801–17.

DeLong R, Reynolds CM, Malcom Y, Schaeffer A, Severs T, Wanekaya A. 2010. Functionalized gold nanoparticles for the binding, stabilization, and delivery of therapeutic dna, rna, and other biological macromolecules. *Nanotechnol. Sci. Appl.* 3:53–63.

Doody JF, Wang Y, Patel SN, Joynes C, Lee SP, Gerlak J, Rolser RL, Li Y, Steiner P, Bassi R, Hicklin DJ, Hadari YR. 2007. Inhibitory activity of cetuximab on epidermal growth factor receptor mutations in non-small cell lung cancer. Mol Cancer Ther. 6:2642-2651.

Dreaden EC, Alkilany AM, Huang X, Murphy CJ, El-Sayed M a. 2012. The golden age: gold nanoparticles for biomedicine. *Chem. Soc. Rev.* 41(7):2740–79.

Egusquiaguirre SP, Igartua M, Hernández RM, Pedraz JL. 2012. Nanoparticle delivery systems for cancer therapy: advances in clinical and preclinical research. *Clin. Transl. Oncol.* 14(2):83–93.

Ernst O, Zor T. 2010. Linearization of the bradford protein assay. *J. Vis. Exp.*, pp. 1–6

Fakruddin M, Hossain Z, Afroz H. 2012. Prospects and applications of nanobiotechnology: a medical perspective. *J. Nanobiotechnology*. 10(31):8 pages.

Fischer MJE. 2010. Amine coupling through edc/nhs: a pratical approach. In *Surface Plasmon Resonance*, ed NJ Mol, MJE Fischer. 627:55–74. Totowa, NJ: Humana Press.

Forman D, de Martel C, Lacey CJ, Soerjomataram I, Lortet-Tieulent J, et al. 2012. Global burden of human papillomavirus and related diseases. *Vaccine*. 30S:F12–23.

Frezza M, Hindo S, Chen D, Davenport A, Schmitt S, et al. 2010. Novel metals and metal complexes as platforms for cancer therapy. *curr pharm des*. 16(16):1813–25.

Gianferrara T, Bratsos I, Alessio E. 2009. A categorization of metal anticancer compounds based on their mode of action. *Dalton Trans.*, pp. 7588–98.

Giljohann D a, Seferos DS, Daniel WL, Massich MD, Patel PC, Mirkin C a. 2010. Gold nanoparticles for biology and medicine. *Angew. Chemie*. 49:3280–94.

GLOBOCAN 2012. http://globocan.iarc.fr/ (accessed in January, 2014).

Goode EL, Ulrich CM, Potter JD. 2002. Polymorphisms in dna repair genes and associations with cancer risk. *Cancer Epidemiol. biomarkers Prev.* 11:1513–30.

Gordon RR, Nelson PS. 2012. Cellular senescense and cancer chemotherapy resistance. *drug Resist. Updat.* 15(1-2):123–31.

Gu Y-J, Cheng J, Man CW-Y, Wong W-T, Cheng SH. 2012. Gold-doxorubicin nanoconjugates for overcoming multidrug resistance. *Nanomedicine*. 8:204–11.

Hadjiandreou MM, Mitsis GD. 2013. Taking a break from chemotherapy to fight drug-resistance: the cases of cancer and hiv/aids. *35th Annu. Int. Conf. IEEE Eng. IEEE EMBS*, pp. 197–200.

Hanahan D, Weinberg RA. 2000. The hallmarks of cancer. *Cell*. 100:57–70.

Hanahan D, Weinberg R a. 2011. Hallmarks of cancer: the next generation. *Cell*. 144(5):646–74.

Helleday T, Petermann E, Lundin C, Hodgson B, Sharma RA. 2008. Dna repair pathways as targets for cancer therapy. *Nat. Rev. - Cancer*. 8:193–204.

Heo DN, Yang DH, Moon H-J, Lee JB, Bae MS, et al. 2012. Gold nanoparticles surface-functionalized with paclitaxel drug and biotin receptor as theranostic agents for cancer therapy. *Biomaterials*. 33:856–66.

Horiba Scientific, Dynamic Light Scattering Technology. http://www.horiba.com/ (accessed in July, 2014).

Housni A, Ahmed M, Liu S, Narain R. 2008. Monodisperse protein stabilized gold nanoparticles via a simple photochemical process. *J. Phys. Chem. C*. 112(32):12282–90.

Hsu Y-F, Ajona D, Corrales L, Lopez-Picazo JM, Gurpide A, Montuenga LM, Pio R. 2010. Complement activation mediates cetuximab inhibition of non-small cell lung cancer tumor growth *in vivo*. *Molecular Cancer*. 9:8 pages.

Ichihara E, Kiura K, Tanimoto M. 2011. Targeting angiogenesis in cancer therapy. *Acta Med. Okayama*. 65(6):353–62.

Irigaray P, Newby J a, Clapp R, Hardell L, Howard V, et al. 2007. Lifestyle-related factors and environmental agents causing cancer: an overview. *Biomed. Pharmacother.* 61(10):640–58.

Iris Biotech GMBH, Reagents. http://www.iris-biotech.de/ (accessed in July, 2014).

Irish Cancer Society, Cancer information, Treatments. http://www.cancer.ie/ (accessed in March, 2014).

Jabir NR, Tabrez S, Ashraf GM, Shakil S, Damanhouri G a, Kamal M a. 2012. Nanotechnology-based approaches in anticancer research. *Int. J. Nanomedicine*. 7:4391–4408.

Jemal A, Bray F, Ferlay J. 2011. Global cancer statistics. . 61(2):69–90.

Kamal JKA, Behere D V. 2005. Binding of heme to human serum albumin: steady-state fluorescence, circular dichroism and optical difference spectroscopic studies. *Indian J. Biochem. Biophys.* 42(1):7–12.

Khullar P, Singh V, Mahal A, Dave PN, Thakur S, et al. 2012. Bovine serum albumin bioconjugated gold nanoparticles: synthesis, hemolysis, and cytotoxicity toward cancer cell lines. *J. Phys. Chem. C*. 116:8834–43.

Kim E-S, Ahn EH, Chung E, Kim D-H. 2013. Recent advances in nanobiotechnology and high-throughput molecular techniques for systems biomedicine. *Mol. Cells*. 36:477–84.

Kintalk, Cancer genetics. http://kintalk.org/genetics-101/ (accessed in March, 2014).

Kumar A, Zhang X, Liang X-J. 2013a. Gold nanoparticles: emerging paradigm for targeted drug delivery system. *Biotechnol. Adv.* 31(5):593–606.

Kumar D, Saini N, Jain N, Sareen R, Pandit V. 2013b. Gold nanoparticles: an era in bionanotechnology. *Expert Opin. Drug Deliv.* 10(3):397–409.

Ladj R, Bitar A, Eissa M, Mugnier Y, Le Dantec R, et al. 2013. Individual inorganic nanoparticles: preparation, functionalization and in vitro biomedical diagnostic applications. *J. Mater. Chem. B*. 1:1381–96.

Lahtz C, Pfeifer GP. 2011. Epigenetic changes of dna repair genes in cancer. *J. Mol. Cell Biol.* 3(1):51–58.

Lakowicz JR. 2006. Protein fluorescence. In *Principles of Fluorescence Spectroscopy*, pp. 529–75.

Lal H, Kolaja KL, Force T. 2013. Cancer genetics and the cardiotoxicity of the therapeutics. *J. Am. Coll. Cardiol.* 61(3):267–74.

Lee C, Meisel D. 1982. Adsorption and surface-enhanced raman of dyes on silver and gold sols'. . 60439(50 mL):3391–95.

Lewis B. 2004. Oncogenes and cancer. In *Genes VIII*, pp. 889–937.

Lien Nghiem TH, Nguyen TT, Fort E, Nguyen TP, Nhung Hoang TM, et al. 2012. Capping and in vivo toxicity studies of gold nanoparticles. *Adv. Nat. Sci. Nanosci. Nanotechnol.* 3:5 pages.

Longley DB, Johnston PG. 2005. Molecular mechanisms of drug resistance. *J. Pathol.* 205(2):275–92.

Luís DV. 2011. Caracterização do efeito anti-tumoral de complexos organometálicos contendo 1,10-fenantrolina-5,6-diona. *Master Thesis, FCT-UNL.*

Luís DV, Silva J, Tomaz AI, de Almeida RFM, Larguinho M, et al. 2014. Insights into the mechanisms underlying the antiproliferative potential of a co(ii) coordination compound bearing 1,10-phenanthroline-5,6-dione: dna and protein interaction studies. *J. Biol. Inorg. Chem.* 19(6):787-803.

Ma P, Mumper RJ. 2013. Paclitaxel nano-delivery systems: a comprehensive review. *J. Nanomed. Nanotechnol.* 4(2):16 pages.

Macciò A, Madeddu C. 2013. Cisplatin : an old drug with a newfound efficacy - from mechanisms of action to cytotoxicity. *Expert Opin. Pharmacother.* 14(13):1839–57.

Martins P, Marques M, Coito L, Pombeiro AJL, Baptista PV, Fernandes AR. 2014a. Organometallic compounds in cancer therapy: past lessons and future directions. Anti-cancer agents in medicinal chemistry. 1871-5206.

Martins P, Rosa D, Fernandes AR, Baptista P V. 2014b. Nanoparticle drug delivery systems : recent patents and applications in nanomedicine. *Recent Patents Nanomed.* 3(2):105-118.

Murawala P, Tirmale A, Shiras A, Prasad BL V. 2014. In situ synthesized bsa capped gold nanoparticles: effective carrier of anticancer drug methotrexate to mcf-7 breast cancer cells. *Mater. Sci. Eng.* 34:158–67.

Murawska M, Skrzypczak A, Kozak M. 2012. Structure and morphology of gold nanoparticles in solution studied by tem , saxs and uv-vis.121(4):888–92.

Naahidi S, Jafari M, Edalat F, Raymond K, Khademhosseini A, Chen P. 2013. Biocompatibility of engineered nanoparticles for drug delivery. *J. Control. release*. 166:182–94.

Negrini S, Gorgoulis VG, Halazonetis TD. 2010. Genomic instability - an evolving hallmark of cancer. *Nat. Rev. Mol. Cell Biol.* 11(3):220–28.

Negrini S, Prada I, D'Alessandro R, Meldolesi J. 2013. Rest: an oncogene or a tumor suppressor? *Cell Trends cell Biol.* 23(6):289–95.

Nowell PC, Hungerford DA. 1960. Chromosome studies on normal and leukemic human leukocytes. *J. Natl. cancer Inst.* 25:85–109.

Nygård M, Hansen BT, Dillner J, Munk C, Oddsson K, et al. 2014. Targeting human papillomavirus to reduce the burden of cervical, vulvar and vaginal cancer and pre-invasive neoplasia: establishing the baseline for surveillance. *PLoS One*. 9(2):9 pages.

Parveen S, Misra R, Sahoo SK. 2012. Nanoparticles: a boon to drug delivery, therapeutics, diagnostics and imaging. *Nanomedicine*. 8(2):147–66.

Perez-Torres M, Guix M, Gonzalez A, Arteaga CL. 2006. Epidermal growth factor receptor (EGFR) antibody down-regulates mutant receptors and inhibits tumors expressing EGFR mutations. *The Journal Of Biological Chemistry*. 281(52):40183-40192.

Pizarro AM, Habtemariam A, Sadler PJ. 2010. Activation mechanisms for organometallic anticancer complexes. *top organomet chem*. 32:21–56.

Podlaha O, Riester M, De S, Michor F. 2012. Evolution of the cancer genome. *Cell Trends Genet.* 8(4):155–63.

Rahme K, Chen L, Hobbs RG, Morris M a., O'Driscoll C, Holmes JD. 2013. Pegylated gold nanoparticles: polymer quantification as a function of peg lengths and nanoparticle dimensions. *RSC Adv.* 3:6085-6094.

Romero-Canelón I, Sadler PJ. 2013. Next-generation metal anticancer complexes: multitargeting via redox modulation. *Inorg. Chem.* 52(21):12276–91.

Sankareswari VG, Vinod D, Mahalakshmi A, Alamelu M, Kumaresan G, et al. 2014. Interaction of oxovanadium(iv)-salphen complexes with bovine serum albumin and their cytotoxicity against cancer. *Dalt. Trans.* 43:3260–72.

Santos GC, Shepherd FA, Tsao MS. 2011. EGFR mutations and lung cancer. *Annu Ver Pathol Mech Dis*. 6:49-69.

Sanz Mendiguchia B, Pucci D, Mastropietro TF, Ghedini M, Crispini A. 2013. Non-classical anticancer agents: on the way to water soluble zinc(ii) heteroleptic complexes. *Dalt. Trans.* 42(19):6768–74.

Schmitt sara m, Frezza M, Dou Q ping. 2012. New applications of old metal-binding drugs in the treatment of human cancer. *Front biosci*. 4:375–91.

Selgrad M, Bornschein J, Rokkas T, Malfertheiner P. 2012. Helicobacter pylori: gastric cancer and extragastric intestinal malignancies. *Helicobacter*. 17 Suppl 1:30–35.

Seyfried TN, Huysentruyt LC. 2013. On the origin of cancer metastasis. *Crit. Rev. Oncog.* 18(1-2):43–73.

Shahabadi N, Maghsudi M, Ahmadipour Z. 2012. Study on the interaction of silver(i) complex with bovine serum albumin by spectroscopic techniques. *Spectrochim. Acta. A. Mol. Biomol. Spectrosc.* 92:184–88.

Shi X, Li D, Xie J, Wang S, Wu Z, Chen H. 2012. Spectroscopic investigation of the interactions between gold nanoparticles and bovine serum albumin. *Chinese Sci. Bull.* 57(10):1109–15.

Silva A, Luís D, Santos S, Silva J, Mendo AS, et al. 2013a. Biological characterization of the antiproliferative potential of co(ii) and sn(iv) coordination compounds in human cancer cell lines: a comparative proteomic approach. *Drug Metabol. Drug Interact.* 28(3):167–76.

Silva J, Fernandes AR, Baptista PV. 2014c. Application of nanotechnology in drug delivery. In *Application of nanotechnology in drug delivery*, ed Sezer AD. ISBN 978-953-51-1628-8.

Silva T, Smoleński P, Martins LMDRS, Guedes da Silva MFC, Fernandes AR, et al. 2013b. Cobalt and zinc compounds bearing 1,10-phenanthroline-5,6-dione or 1,3,5-triaza-7-phosphaadamantane derivatives - synthesis, characterization, cytotoxicity, and cell selectivity studies. *Eur. J. Inorg. Chem.*, pp. 3651–58.

Stephan C, Hineman A. 2012. *Analysis of NIST Gold Nanoparticles Reference Materials Using the NexION 300 ICP-MS in Single Particle Mode*. Perkin Elmer.

Tayeh N, Rungassamy T, Albani JR. 2009. Fluorescence spectral resolution of tryptophan residues in bovine and human serum albumins. *J. Pharm. Biomed. Anal.* 50:107–16.

Thompson D. 2007. Michael faraday ' s recognition of ruby gold : the birth of modern nanotechnology. *Gold Bull.* 40(4):267–69.

Tiwari P, Vig K, Dennis V, Singh S. 2011a. Functionalized gold nanoparticles and their biomedical applications. *Nanomaterials*. 1:31–63.

Torchilin VP. 2010. Passive and active drug targeting: drug delivery to tumors as an example. In *Drug delivery*, ed M Schäfer-Korting. 197:3–53. Berlin, Heidelberg: Springer Berlin Heidelberg.

Tran N, Webster TJ. 2013. Understanding magnetic nanoparticle osteoblast receptor-mediated endocytosis using experiments and modeling. *Nanotechnology*. 24(18):185102.

Trivedi N, Patel N, Upadhyay UM, Shah V. 2012. Gold nanoparticulate drug delivery system : a review. *Int. J. Compr. Pharm.* 02(03):1–5.

Trnková L, Boušová I, Kubí V, Dršata J. 2010. Binding of naturally occurring hydroxycinnamic acids to bovine serum albumin. *Nat. Sci.* 2(6):563–70.

Varlan A, Hillebrand M. 2010. Bovine and human serum albumin interactions with 3-carboxyphenoxathiin studied by fluorescence and circular dichroism spectroscopy. *Molecules*. 15:3905–19.

Vivian JT, Callis PR. 2001. Mechanisms of tryptophan fluorescence shifts in proteins. *Biophys. J.* 80:2093–2109.

Vlasova IM, Saletsky AM. 2009. Study of the denaturation of human serum albumin by sodium dodecyl sulfate using the intrinsic fluorescence of albumin. 76(4):536–41.

Voliani V, Signore G, Nifosí R, Ricci F, Luin S, Beltram F. 2012. Smart delivery and controlled drug release with gold nanoparticles : new frontiers in nanomedicine. *Recent Patents Nanomed.* 2:34–44.

Wang AZ, Langer R, Farokhzad OC. 2012. Nanoparticle delivery of cancer drugs. *Annu. Rev. Med.* 63:185–98.

World Health Organization, Cancer. http://www.who.int/en/ (accessed in March, 2014)

Wroblewski LE, Peek RM, Wilson KT. 2010. Helicobacter pylori and gastric cancer: factors that modulate disease risk. *Clin. Microbiol. Rev.* 23(4):713–39.

Xu H, Yao N, Xu H, Wang T, Li G, Li Z. 2013. Characterization of the interaction between eupatorin and bovine serum albumin by spectroscopic and molecular modeling methods. *Int. J. Mol. Sci.* 14:14185–203.

Yadav A, Ghune M, Jain DK. 2011. Nano-medicine based drug delivery system. *J. Adv. Pharm. Educ. Res.* 1(4):201–13.

Yang L, Han Y, Suarez Saiz F, Minden MD. 2007. A tumor suppressor and oncogene: the wt1 story. *Leukemia*. 21:868–76.

Yohannes G, Wiedmer SK, Elomaa M, Jussila M, Aseyev V, Riekkola M-L. 2010. Thermal aggregation of bovine serum albumin studied by asymmetrical flow field-flow fractionation. *Anal. Chim. Acta*. 675:191–98.

Yokoyama K, Asakura T, Nakamura N, Ohno H. 2006. Chemical modification of cytochrome c by a ruthenium complex containing phenanthroline quinone. *Inorg. Chem. Commun.* 9:281–83.

## VI. APPENDICES

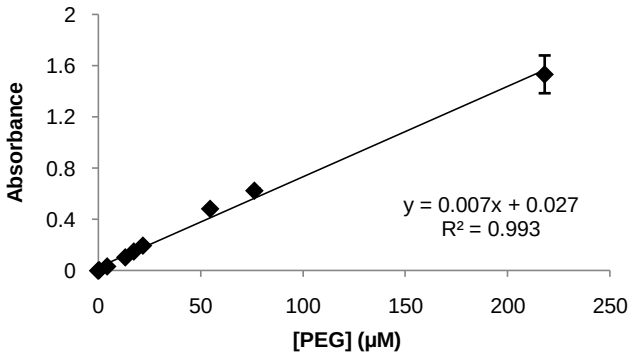


Figure VI.1 – Linear standard curve in the range of 0 – 0.5 mg/mL of PEG, measured at the wavelength of 412 nm by UV-Vis spectroscopy. This standard curve supports the Ellman's method and the quantification of thiolated chains per AuNP was determined after interpolation. The linear range is given by the following equation: Abs412 nm = 0.007x[PEG, µM] + 0.027. The data is relative to the mean of three independent assays and error bars are correspondent to SEM.

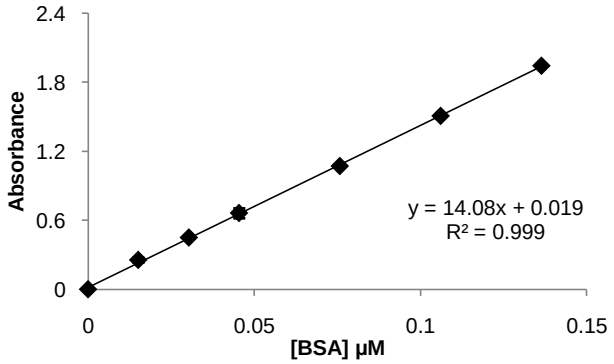


Figure VI.2 – Linear standard curve in the range of 0 – 0.14 µM of BSA obtained by UV-Vis spectroscopy. This standard curve supports the Bradford assay and the quantification of BSA per AuNP was determined after interpolation. The linear range is given by the following equation: Abs(595/450)nm = 14.08x[BSA, µM] + 0.019. The data is relative to the mean of three independent assays and error bars are correspondent to SEM.

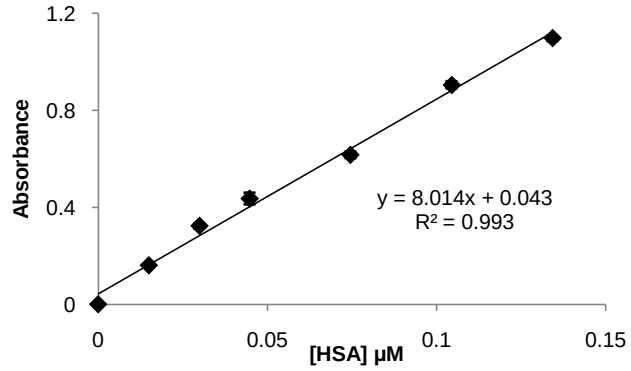


Figure VI.3 – Linear standard curve in the range of 0 – 0.14 µM of HSA obtained by UV-Vis spectroscopy. This standard curve supports the Bradford assay and the quantification of HSA per AuNP was determined after interpolation. The linear range is given by the following equation:

Abs(595/450)nm = 8.014x[HSA, µM] + 0.043. The data is relative to the mean of three independent assays and error bars are correspondent to SEM.

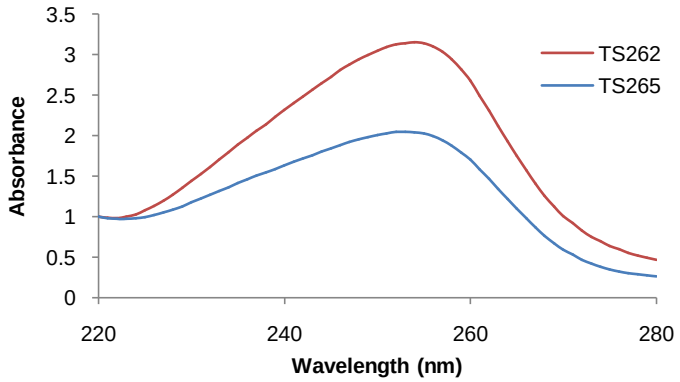


Figure VI.4 – Spectra corresponding to the maximum absorbance wavelengths of TS262 and TS265 compounds – 254 and 253 nm, respectively – obtained by UV-Vis spectroscopy in the range frequency of 200 - 280 nm, in a milli-Q $H_2O$ solution.

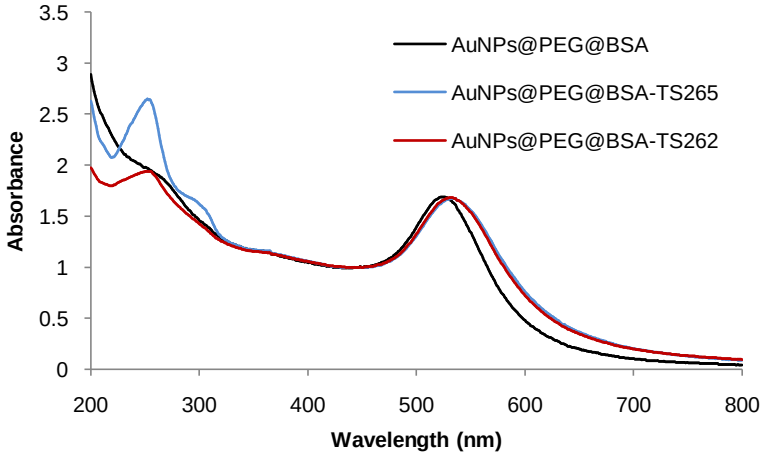


Figure VI.5 – Spectra corresponding to the AuNPs@PEG@BSA, AuNPs@PEG@BSA-TS262, AuNPs@PEG@BSA-TS265, obtained by UV-Vis spectroscopy in the range frequency of 200 - 800 nm, in a pH 7.0 solution. The maximum absorbance peak at 254 nm and 253 nm can confirmed the presence of TS262 and TS265, respectively, on AuNPs surface.

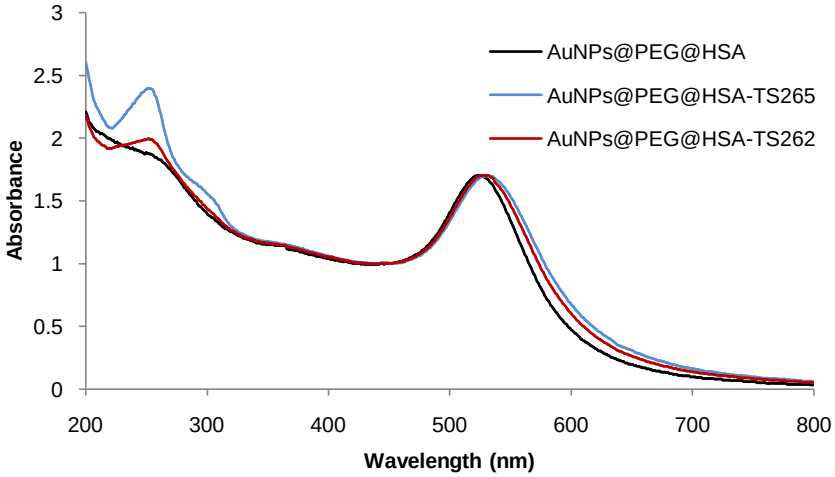


Figure VI.6 – Spectra corresponding to the AuNPs@PEG@HSA, AuNPs@PEG@HSA-TS262, AuNPs@PEG@HSA-TS265, obtained by UV-Vis spectroscopy in the range frequency of 200 - 800 nm, in a pH 7.0 solution. The maximum absorbance peak at 254 nm and 253 nm can confirmed the presence of TS262 and TS265, respectively, on AuNPs surface.

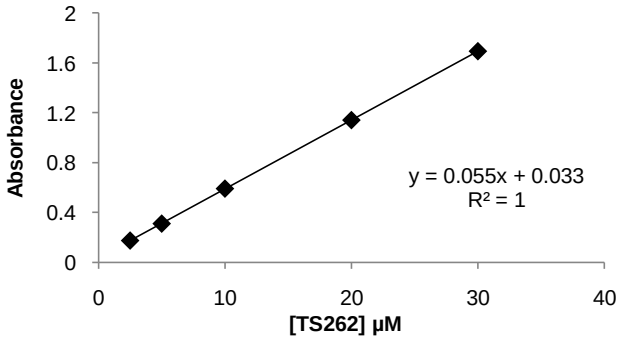


Figure VI.7 – Standard curve in the range of 2.5 – 30 µM of TS262, measured at the wavelength of 254 nm by UV-Vis spectroscopy. It allows the determination of the TS262 molar extinction coefficient through Lamber-Beer law, and was determined in 55300 $M^{-1}$ $cm^{-1}$.

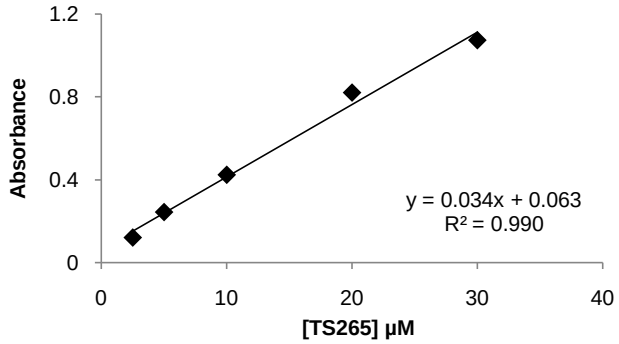


Figure VI.8 – Standard curve in the range of 2.5 – 30 µM of TS265, measured at the wavelength of 253 nm by UV-Vis spectroscopy. It allows the determination of the TS265 molar extinction coefficient through Lamber-Beer law, and was determined in 34900 $M^{-1}$ $cm^{-1}$.